

This work was written as part of one of the author's official duties as an Employee of the United States Government and is therefore a work of the United States Government. In accordance with 17 U.S.C. 105, no copyright protection is available for such works under U.S. Law.

Public Domain Mark 1.0

<https://creativecommons.org/publicdomain/mark/1.0/>

Access to this work was provided by the University of Maryland, Baltimore County (UMBC) ScholarWorks@UMBC digital repository on the Maryland Shared Open Access (MD-SOAR) platform.

**Please provide feedback**

Please support the ScholarWorks@UMBC repository by emailing [scholarworks-group@umbc.edu](mailto:scholarworks-group@umbc.edu) and telling us what having access to this work means to you and why it's important to you. Thank you.

# JGR Atmospheres

## RESEARCH ARTICLE

10.1029/2018JD029598

### Key Points:

- VIIRS and MODIS Deep Blue show very similar validation results against AERONET
- Decadal stability in retrieved AOD is about 0.01 per decade or better
- The data sets show consistent seasonal and interannual variations in regional AOD

### Supporting Information:

- Supporting Information S1
- Data Set S1

### Correspondence to:

A. M. Sayer,  
andrew.sayer@nasa.gov

### Citation:

Sayer, A. M., Hsu, N. C., Lee, J., Kim, W. V., & Dutcher, S. T. (2019). Validation, stability, and consistency of MODIS collection 6.1 and VIIRS version 1 Deep Blue aerosol data over land. *Journal of Geophysical Research: Atmospheres*, 124, 4658–4688. <https://doi.org/10.1029/2018JD029598>

Received 31 AUG 2018

Accepted 23 FEB 2019

Accepted article online 4 MAR 2019

Published online 24 APR 2019

### Author Contributions

**Conceptualization:** Andrew M. Sayer, N. Christina Hsu  
**Data curation:** Steven T. Dutcher  
**Funding Acquisition:** Andrew M. Sayer, N. Christina Hsu, Jaehwa Lee  
**Methodology:** Andrew M. Sayer  
**Software:** Andrew M. Sayer  
**Validation:** Andrew M. Sayer  
**Writing - Original Draft:** Andrew M. Sayer  
**Formal Analysis:** Andrew M. Sayer  
**Investigation:** Andrew M. Sayer, N. Christina Hsu, Jaehwa Lee, Woogyung V. Kim  
**Project Administration:** N. Christina Hsu  
**Resources:** Steven T. Dutcher  
**Supervision:** N. Christina Hsu  
**Visualization:** Andrew M. Sayer  
**Writing - review & editing:** N. Christina Hsu, Jaehwa Lee, Woogyung V. Kim, Steven T. Dutcher

©2019. American Geophysical Union.  
All Rights Reserved.

## Validation, Stability, and Consistency of MODIS Collection 6.1 and VIIRS Version 1 Deep Blue Aerosol Data Over Land

Andrew M. Sayer<sup>1,2</sup> , N. Christina Hsu<sup>2</sup> , Jaehwa Lee<sup>2,3</sup> , Woogyung V. Kim<sup>2,3</sup> , and Steven T. Dutcher<sup>4</sup>

<sup>1</sup>Goddard Earth Sciences Technology And Research (GESTAR), Universities Space Research Association, Greenbelt, MD, USA, <sup>2</sup>Climate and Radiation Laboratory, NASA Goddard Space Flight Center, Greenbelt, MD, USA, <sup>3</sup>Earth System Science Interdisciplinary Center, University of Maryland, College Park, MD, USA, <sup>4</sup>Atmosphere SIPS, Space Science and Engineering Center, University of Wisconsin-Madison, Madison, WI, USA

**Abstract** The Deep Blue (DB) algorithm has been used to retrieve aerosol optical depth (AOD) and Ångström exponent (AE) over land from multiple satellite instruments, including the Moderate Resolution Imaging Spectroradiometers (MODIS) aboard the Terra and Aqua platforms and the Visible Infrared Imaging Radiometer Suite (VIIRS). This study first validates the latest MODIS (Collection 6.1) and VIIRS (Version 1) DB data products against Aerosol Robotic Network observations. On global average, the typical level of uncertainty in AOD is slightly better than  $\pm(0.05 + 20\%)$  relative to Aerosol Robotic Network. AE is quantitatively more uncertain but qualitatively shows skill at distinguishing between fine-mode and coarse-mode dominated aerosol columns. Results are also compared with the previous MODIS Collection 6. The stability of the three DB data sets ranges from 0.005–0.01 AOD per decade. Second, spatial and temporal patterns in AOD and AE are compared between the three data sets. It is found that they all show similar patterns of spatial coverage, which is predominantly linked to cloud cover, snow, and polar night. Regional time series of AOD also show highly consistent seasonal and interannual variations and are strongly correlated, although have offsets in some regions due to a combination of algorithmic and sensor-related differences.

**Plain Language Summary** Aerosols are small particles in the atmosphere like desert dust, volcanic ash, smoke, industrial haze, and sea spray. Understanding them is important for applications such as hazard avoidance, air quality and human health, and climate studies. Satellite instruments provide an important tool to study aerosol loading over the world. However, individual satellites do not last forever, and newer satellites often have improved capabilities compared to older ones. This paper evaluates the latest version of the Deep Blue algorithm for monitoring aerosols as applied to the Moderate Resolution Imaging Spectroradiometers (MODIS) and Visible Infrared Imaging Radiometer Suite (VIIRS) satellite instruments. The two MODIS sensors provide data from 2000 and 2002 onward, while the first VIIRS was launched in late 2011, and VIIRS will carry on the MODIS data records into the future. The evaluation is performed by comparing to ground-truth data which are part of (National Aeronautics and Space Administration) NASA's global Aerosol Robotic Network. The stability in time and consistency between the MODIS and VIIRS data sets are also examined.

## 1. Introduction

The Deep Blue (DB) algorithm was initially developed to retrieve aerosol properties above bright reflecting surfaces such as deserts, bare soil, and urban areas from spaceborne imaging radiometers (Hsu et al., 2004, 2006). The primary quantity retrieved by DB is the total column aerosol optical depth (AOD) at 550 nm. Secondary quantities are AOD at various other wavelengths in the visible spectral region and the Ångström exponent (AE), which is related to the optical dominance of fine versus coarse aerosol particles in the column, as well as to the sizes of the particles within fine and coarse modes (Eck et al., 1999; Schuster et al., 2006). A main motivation behind the development of DB was that prior Dark Target (DT) types of algorithm developed for single-view satellite sensors exhibit significant error in these regions (Levy et al., 2010). This is because the spectral relationships they assume between surface reflectance at different bands, developed based on assumptions of vegetation-dominated scenes, are significantly more uncertain for these surface

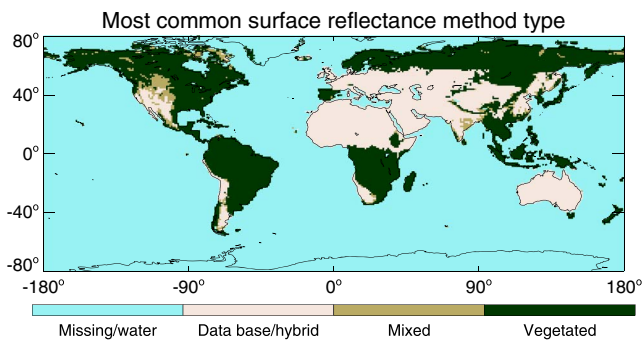


**Figure 1.** Most common surface reflectance method applied in VIIRS DB retrievals from the year 2014: data base (including hybrid AERONET BRDF scaling), vegetated BRDF, or mixed. Data shown aggregated to 1° horizontal resolution; grid cells with fewer than 10 retrievals total, typically from water or snow cover, are shaded in pale blue.

types (Kaufman et al., 1997; Levy et al., 2007). Thus, over-land DT algorithms such as applied to Moderate Resolution Imaging Spectroradiometer (MODIS) measurements aboard the Terra and Aqua satellites had systematic positive offsets in mountains and built-up areas and did not provide coverage over bright deserts (Levy et al., 2010; Remer et al., 2008). This is an important missing piece of the global aerosol system, as deserts are the main source of mineral dust aerosols, which are transported long distances and affect the global climate system significantly (e.g., Heald et al., 2014; Koren et al., 2006; Prospero et al., 2014), and without near-source observations, it is difficult to constrain source strengths from remote sensing.

In the blue spectral region ( $\sim 412\text{--}490\text{ nm}$ ), the surface reflectance is (except for snow) comparatively dark, homogeneous on spatial scales similar to satellite pixel sizes, and has limited temporal variability relative to vegetated surfaces (Hsu et al., 2004, 2006). The darkness increases the contrast between surface features and atmospheric aerosols, and the temporal stability increases the robustness of this contrast. DB was therefore

developed by first creating a surface reflectance data base from atmospherically corrected satellite observations in those regions where DT methods did not work well. Then, using an assumed aerosol optical model and with the data base as a constraint, AOD and AE can be retrieved pixel-by-pixel. Initial DB development was done using measurements from the Sea-viewing Wide Field-of-view Sensor (SeaWiFS) and MODIS. Beginning in Collection 5 (C5), DB retrievals were included within the MODIS Atmospheres data product suite alongside DT land and ocean aerosol products. This included a full-mission reprocessing and routine forward processing for measurements from both the Terra (2000 onward) and Aqua (2002 onward) platforms. Inclusion of DB greatly increased the spatial coverage of aerosol data available from such single-view broad-swath imagers and has benefited studies assessing the global aerosol burden, particularly in regard to dust (e.g., Chin et al., 2014; Ginoux et al., 2012; Ridley et al., 2016; van Donkelaar et al., 2016).

Following this, a second-generation DB algorithm was developed with the goal of expanding coverage from bright surfaces to all snow-free land surfaces (Hsu et al., 2013). This was achieved by developing new spectral-directional relationships for vegetated surface reflectance, similar in principle to the DT approach but with additional stratification by scene Normalized Difference Vegetation Index (NDVI), geometry, and subcategories of cover type (e.g., croplands vs. forests) to give a bidirectional reflectance distribution function (BRDF) model. An algorithm flag was introduced into the data to identify whether the data base or vegetated BRDF method was applied for a given pixel. For some parts of the world, additional BRDF shapes were developed based on atmospheric correction using Aerosol Robotic Network (AERONET) AOD data (Hsu et al., 2013). These BRDFs were applied as a scaling factor to the surface data base, as a hybrid between the data base and vegetated techniques. In the DB algorithm flag, this third AERONET-based BRDF subset of retrievals is grouped together with the standard data base method retrievals in the data products.

The determination of data base versus vegetated method for estimating surface reflectance is made on a pixel-by-pixel basis, but Figure 1 shows the general spatial distribution of these two paths. Generally, the data base method is used over deserts and mountains, which is why this is often referred to as the “arid” or “bright” retrieval path. However, it is important to note that, through the hybrid AERONET BRDF technique, it is also applied in nonarid regions such as much of Europe and South Asia. An additional category within Figure 1 is “mixed,” corresponding to cases where an individual retrieval contained contributing sensor pixels from both methods, and is most commonly found in transitional regions between the other two classes.

Additional refinements were made to surface data base creation, cloud screening, quality assurance (QA) tests, and aerosol optical models, addressing limitations found in C5 (Sayer et al., 2013). By this time, the blue bands for MODIS aboard the Terra satellite had begun to degrade significantly, and so corrections to sensor response versus scan angle, gain, and polarization sensitivity, initially developed for ocean color processing (Meister & Franz, 2011; Meister et al., 2005), were implemented to allow MODIS Terra DB processing to continue (Jeong et al., 2011; Sayer, Hsu, Bettenhausen, Jeong, & Meister, 2015). For MODIS, prognos-

tic retrieval-level uncertainty estimates were developed and implemented as an aid to data assimilation applications (Sayer et al., 2013).

Data processed with this second-generation algorithm were released in 2012, for SeaWiFS and MODIS, keeping algorithms as consistent as practical given sensor differences. Validation showed that the two had similar overall quality (Sayer et al., 2013; Sayer, Hsu, Bettenhausen, Jeong, et al., 2012). The SeaWiFS data set also included a Satellite Ocean Aerosol Retrieval (SOAR) algorithm (Sayer, Hsu, Bettenhausen, Ahmad, et al., 2012), providing coverage over-water surfaces. SOAR was not applied to MODIS due to the prior existence of a MODIS DT over-water algorithm (Tanré et al., 1997). In this new MODIS Collection 6 (C6), a merged DB-DT data set was also provided (Sayer, Munchak, et al., 2014), taking advantage of the coverage and relative strengths provided from both the second-generation DB (Hsu et al., 2013) and updated DT (Levy et al., 2007) algorithms.

After this, two parallel efforts continued. One was an application to Advanced Very High Resolution Radiometer (AVHRR) measurements, which could in principle extend the time series to 1979. Although the AVHRRs lacked bands at blue wavelengths, it was found that over many semiarid surfaces, the surface data base approach could still perform well and that NDVI-based approaches could be used to constrain surface reflectance for AOD retrieval over vegetated surfaces (Hsu et al., 2017). Data from three of the AVHRR sensors were processed and validated using AERONET and ship-based measurements, and the retrievals found to perform with the expected levels of uncertainty and consistency with SeaWiFS and MODIS results (Sayer, Hsu, Lee, et al., 2017).

In late 2011, the Visible Infrared Imaging Radiometer Suite (VIIRS) was launched on the Suomi-National Polar-orbiting Partnership (S-NPP) satellite. S-NPP is the precursor to a new series of operational U.S. polar-orbiting satellites, and the second effort has been to adapt DB and SOAR for application to VIIRS measurements. This will enable the DB/SOAR data record to continue following the loss of the SeaWiFS sensor (1997–2010) and anticipated end of the current MODIS Terra/Aqua and AVHRR missions over the coming years.

A MODIS Atmospheres Collection 6.1 (C6.1) was released in 2017. While this effort was initiated primarily by the need to fix a crosstalk issue in some of MODIS Terra's thermal bands (Moeller et al., 2017), it provided an opportunity for further refinements to the basic DB approach from C6 (mainly updates to thresholds and aerosol optical models addressing remaining known issues in C6). One further update is that corrections for sensor response versus scan angle and polarization degradation, previously applied only to MODIS Terra data (Sayer, Hsu, Bettenhausen, Jeong, & Meister, 2015), are now also applied to MODIS Aqua, as that sensor was also found to be deteriorating. This C6.1 algorithm is also the basis for the VIIRS DB data set. Specific changes between the C6 and C6.1 algorithms, and a general description of the new VIIRS DB Version 1 (V1) data set, will be described in a separate study; the VIIRS application of SOAR is also described elsewhere (Sayer et al., 2018).

The purpose of this study is to evaluate the over-land AOD and AE retrievals within the MODIS DB C6.1 and VIIRS DB V1 data sets, through comparison with AERONET reference data, as well as assessing the level of stability and consistency between retrievals from the three platforms (MODIS Terra, Aqua, and VIIRS). MODIS C6.1 and VIIRS V1 data are freely available for download from the NASA Level-1 and Atmosphere Archive and Distribution System website (<https://ladsweb.nascom.nasa.gov>).

## 2. Description of Levels 2 and 3 DB Data Products

MODIS and VIIRS are both single-view broad-swath passive multispectral imaging radiometers, measuring reflected solar and emitted thermal radiation from the visible to thermal infrared spectral regions (Barnes et al., 1998; Cao et al., 2013). They are in Sun-synchronous polar orbits, with daytime local solar crossing times at the Equator of 10:30 for MODIS aboard the Terra platform and ~13:30 for MODIS Aqua and S-NPP VIIRS. Note that Aqua and S-NPP are at different altitudes and on different orbit tracks, so near-simultaneous measurements of the same area are only obtained over portions of the world every several days (Sayer, Hsu, Bettenhausen, et al., 2017), despite the similarity in Equatorial crossing times.

Both sensors have onboard on-orbit calibration and also use the Moon as an additional periodic calibration resource, to monitor and maintain stability (Sun et al., 2007; Toller et al., 2013; Xiong et al., 2016). Native pixel sizes for bands used in DB processing vary between 250 m and 1 km at nadir for MODIS and ~740 m



for VIIRS. Away from nadir views, the sensor scan geometries and Earth's curvature cause a “bow-tie distortion” where pixels become larger, and consecutive scans begin to overlap, at larger view zenith angles (Wolfe et al., 2013; Xiong et al., 2006). For MODIS, the distortion at edge of the 2,330-km swath is about a factor of two in the along-track and five in the across-track direction, and overlap is total, which has consequences for AOD retrieval characteristics (Sayer, Hsu, & Bettenhausen, 2015). For VIIRS, an onboard reaggregation and bow-tie deletion system means that distortion is closer to a factor of two and overlap is much smaller (Wolfe et al., 2013), even at the edge of its 3,040-km swath.

DB data products are provided in two main types. Level 2 (L2) products are created by applying the DB retrieval algorithm to granules consisting of level 1b (L1b; calibrated reflectance/radiance) data along the orbit tracks. The granules contain 5 min of data for the MODIS sensors and 6 min for VIIRS. The DB algorithm is applied to data at full L1b resolution but the L2 product provided at a resolution of one retrieval per L1b scan for MODIS and two per scan line for VIIRS. Due to the differing number of detectors and pixel sizes of MODIS and VIIRS, this corresponds to  $\sim 10$  and  $\sim 6$  km nominal horizontal L2 pixel sizes at nadir, respectively.

Each L2 pixel has an assigned QA value, where 0 indicates no retrieval and 1, 2, and 3 indicate poor, medium, and good expected retrieval quality, respectively. Due to different spectral and spatial measurement characteristics, QA assignment tests differ slightly between MODIS and VIIRS, although the premise remains the same. The most common reason for assignment of low QA is suspected potential for cloud contamination (few cloud-free L1b pixels within the L2 pixel, few neighboring L2 pixels with a retrieval, or high heterogeneity of retrieved AOD within the pixel). Through validation against AERONET, Sayer et al. (2013) found that there was little difference between error characteristics of MODIS DB retrievals assigned QA = 2 or 3, but that QA = 1 had somewhat larger errors. For most purposes, it is recommended that only retrievals with QA  $\geq 2$  are used, and the DB products contain prefiltered data sets, denoted “Best\_Estimate” within the files, according to this recommendation. These are used in the present study.

Level 3 (L3) products are also generated as statistical summaries of the L2 data on a  $1^\circ$  horizontal grid. L3 daily (D3) files are created by aggregating L2 data (using only data with QA  $\geq 2$ ), while L3 monthly (M3) files are aggregates of D3 products. For MODIS, eight-day (E3) aggregated products are also available. Both L2 and L3 products are used in this study. The same types of geophysical parameters are provided for both MODIS and VIIRS in the L2/L3 products.

### 3. Validation With Direct-Sun AERONET Data

Satellite AOD data sets are typically validated using the method of Ichoku et al. (2002). This spatially averages satellite data and temporally averages AERONET data, to account for the fact that AERONET provides point measurements of AOD with a sampling frequency of 5–15 min (dependent on instrument configuration) while satellites provide a snapshot with retrieval footprints covering several to tens of kilometers. This fundamental difference introduces some uncertainty beyond that of AERONET alone, dependent on the heterogeneity in the underlying aerosol field (Virtanen et al., 2018). This analysis uses both an updated AERONET data version and comparison methodology compared to prior DB validation studies so the method used is detailed in full below.

#### 3.1. AERONET Data Description and Matchup Protocol

AERONET uses Sun photometers to infer spectral AOD by direct-Sun observations of solar irradiance, processed in a consistent way, over more than a thousand sites (Holben et al., 1998). The uncertainty on AERONET direct-Sun AOD is  $\sim 0.01$  in the midvisible (Eck et al., 1999), making it a suitable validation resource for satellite remote sensing and model evaluation, for which uncertainties are often considerably larger.

This analysis uses the latest AERONET version 3 direct-Sun L2 (cloud-screened, post-deployment calibrated, and quality-assured; Smirnov et al., 2000) data products. Version 3 includes improvements to sensor characterization and cloud-aerosol discrimination over version 2 (Giles et al., 2019), particularly in the detection of stable optically thin cirrus cloud layers and rapidly evolving fine-mode aerosol plumes. The geolocation accuracy of some sites has also been improved. Here MODIS/VIIRS and AERONET data from all (1,151) sites from the start of the Terra mission until December 2017 are considered; AERONET L2 data

have a latency of several months to years due to the requirement for post-deployment calibration, and so more recent data are at present largely unavailable.

All AERONET instruments provide data at a standard set of wavelengths (440, 675, 870, and 1,020 nm for AOD), and some include additional wavelengths. In this analysis, AERONET AOD are interpolated spectrally to 550 nm, as most AERONET sites do not measure at this band. Previous DB validation studies interpolated using the closest available AERONET wavelength and the AE, where AE (denoted  $\alpha$ ) is defined

$$\alpha = -\frac{d \log(\tau(\lambda))}{d \log(\lambda)} \approx -\frac{\log \frac{\tau_{\lambda_1}}{\tau_{\lambda_2}}}{\log \frac{\lambda_1}{\lambda_2}}, \quad (1)$$

for AOD ( $\tau$ ) around some wavelength  $\lambda$ . Here the spectral interpolation is performed with a least-squares fit of all available AERONET AODs within the 440–870-nm wavelength range (typically 4, more for some configurations) to a quadratic polynomial, as follows (for coefficients  $a_0$ ,  $a_1$ ,  $a_2$  calculated on a point-by-point basis):

$$\log(\tau_\lambda) = a_0 + a_1 \log(\lambda) + a_2 \log(\lambda)^2. \quad (2)$$

This quadratic formulation is more robust to calibration problems in individual channels. It also accounts for the fact that in fine-mode dominant aerosol conditions, the relationship between  $\log(\tau)$  and  $\log(\lambda)$  is not linear but curved, dependent on fine-mode particle size (Eck et al., 1999; Schuster et al., 2006). For low-AOD cases, the difference is negligible so has little effect on the conclusions of prior studies using the simpler (equation (1)) AE. In high-AOD cases dominated by fine-mode aerosols, it results in a better estimate of the true AOD at 550 nm. Hereafter, mentions of AOD without a specified wavelength refer to AOD at 550 nm.

AE is also evaluated in this study. The DB AE wavelength ranges depend on surface type. For retrievals where the surface data base method is used (cf. Figure 1), the wavelength pair 412–470 nm is used for MODIS (412–490 nm for VIIRS, which has a 490 nm band instead of 470 nm), while where the vegetated method is used the AE is defined for 470–650 nm (MODIS) and 490–670 nm (VIIRS). Based on numerical simulations, the differences in MODIS and VIIRS AE resulting from these wavelength differences is expected to be much smaller than the AE retrieval uncertainty and not systematic. This is compared with AERONET AE over the most similar wavelength range, which is typically 440–675 nm but sometimes 440–870 or 500–870 nm when the first choice is absent. If the aerosol column is dominated by mineral dust (as is common over deserts), the difference in wavelength ranges between satellite and AERONET is expected to have negligible impact (as often  $AE \sim 0$  for dust in the visible spectral range). For other aerosol types, there may be more impact, but this is again expected to be smaller than the retrieval uncertainty on this parameter. As AE is a spectral derivative of AOD, when the spectral AOD relative uncertainty is large (e.g., when AOD is low or a surface is quite bright), AE does not have much quantitative value and should more generally be treated as a qualitative parameter.

As in prior studies, DB and AERONET data are compared by averaging satellite retrievals with  $QA \geq 2$  within 25 km of the AERONET site and AERONET data within  $\pm 30$  min of the satellite overpass. To further mitigate inherent differences in the sampling approaches of the two measurement types, two modifications are made to the strategy from prior analyses. The first is that median, rather than mean, values of AOD are reported. This is helpful when, for example, a satellite averaging area includes aerosol plumes which pass near to but not over the AERONET site.

The second is that only aerosol retrievals with a surface elevation within 200 m of the AERONET site are considered, to decrease any systematic sampling biases from differential sampling of the total aerosol column. For example, for a background AOD  $\sim 0.1$  with the bulk of the aerosol within a well-mixed boundary layer of  $\sim 1$  km depth, a Sun photometer situated at 200 m above the nearby surface would miss  $\sim 0.02$  of the AOD, which would lead to an apparent positive bias in the satellite data. Conversely, a Sun photometer in a valley might see more aerosol than a satellite pixel covering mostly areas above a valley, leading to an apparent negative bias in the satellite data. This threshold should ensure that biases from elevation mismatches are unlikely to be much larger than the AERONET AOD uncertainty, which is dominated by radiometric calibration. When AOD is higher, the absolute error induced by this may be higher; although in cases of elevated AOD from transported or lofted aerosols, a large fraction of the AOD may be above the boundary

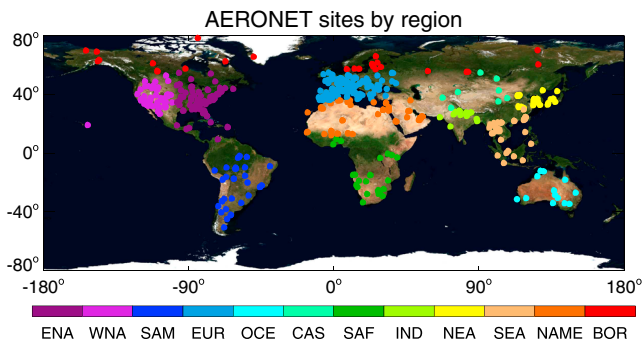


**Figure 2.** Regional assignment for the AERONET sites used in this study, shown for sites with at least 50 matchups in total for at least one of the satellite sensors. Regions are Eastern North America (ENA), Western North America (WNA), South America (SAM), Europe (EUR), Oceania (OCE), Central Asia (CAS), Southern Africa (SAF), Indian subcontinent (IND), Northeastern Asia (NEA), Southeastern Asia (SEA), North Africa/Middle East (NAME), and Boreal (BOR).

layer rather than well-mixed within it. Due to the heterogeneity of land surfaces, in some regions moving to a stricter threshold would significantly decrease the data volume available for comparison, so as with many things, it is a compromise between level of representivity and data coverage. In prior studies, elevation differences have generally not been considered, meaning that these sampling biases are effectively included in the comparison and ascribed to retrieval error. While not important for many sites, this constraint can affect results for sites with complex topography such as mountains/valleys (e.g., Doi Ang Khang, Thailand) or in bowl-shaped depressions (e.g., Mexico City, Mexico).

For VIIRS, L2 pixel-average elevation is provided within the L2 files. For MODIS, it is only provided for pixels where the DT algorithm has a retrieval. As the coverage of DB and DT are different, this is insufficient for the present application. As a result, in this analysis, the Gridded Topography at 30 arc sec resolution (GTOPO30) digital elevation model (Gesch et al., 1999) is used to estimate the elevation of the center of each MODIS L2 pixel, taken as representative. Comparison to available elevations from DT within the MODIS product (where they are available)

gives typical agreement within a few tens of meters, which is in line with the expected  $\pm 30$  m (two standard deviation) uncertainty of GTOPO30 over most terrain types (Gesch & Larson, 1996; Gesch et al., 1999).

A matchup is valid if there is at least one MODIS/VIIRS retrieval in the spatial window and at least one AERONET observation in the temporal window. This results in 891, 832, and 583 sites with matchups for MODIS Terra, MODIS Aqua, and VIIRS, respectively; of these sites, 481, 444, and 384 have at least 50 matchups with these sensors, respectively. A total of 931 sites have matchups with one or more of the sensors. The locations of the 519 sites where at least one sensor has 50 or more matchups are shown in Figure 2 (although note all matchups and all sites are used for the analysis). This reveals that the AERONET network is the densest in North America and Europe.

Ichoku et al. (2002) and others often put a threshold on the minimum number of satellite retrievals or AERONET observations in the averaging window required for a valid matchup. The purpose of this is to decrease the aforementioned inherent differences from the satellite versus ground-based observation types. However, this may introduce additional sampling-related biases into the aggregate statistics, as more heterogeneous (and often difficult-to-retrieve) scenes may be excluded. A danger is that this skews the sample to locations and times of year where features which limit satellite/AERONET data availability (e.g., coastline shape, presence, and structure of cloud fields) are minimized and may therefore provide an unrepresentative assessment of satellite retrieval performance. Here the use of medians and elevation thresholds as above are intended as an alternative approach to filter data while not screening out these more difficult-to-retrieve scenes, providing a more representative picture.

### 3.2. Evaluation Metrics

The main metrics used to evaluate the DB data are as follows:

1. The correlation coefficient, as a measure of how well the satellite data track the variability of the AERONET data. Spearman's rank correlation coefficient is used rather than the more common Pearson's linear correlation coefficient. The reasons for this include the facts that the relationship between AERONET and satellite AOD may not be linear, and also that Spearman's correlation is less sensitive to extreme outliers which may be unrepresentative of the behavior of the data set. These outliers may arise due to, for example, a clean background site having infrequent high-AOD transport events, where these rare events drive up Pearson's correlation coefficient or else sampling mismatches (e.g., high-AOD plumes or cloud contamination in one data set but not the other), which would tend to drive down Pearson's correlation coefficient. Where the true relationship is linear and departures are Gaussian, the two metrics are equivalent.
2. The median (satellite-AERONET) bias between the data sets, as a measure of the general offset. Again, medians are more robust to outliers which can skew the means.
3. The commonly used root mean square error (RMSE). Note that this is dependent upon the typical level of AOD at individual sites as well as the presence of outliers.

**Table 1**

*Global and Regional Statistics for the Satellite Versus Aerosol Robotic Network 550-nm Aerosol Optical Depth Comparison, for Moderate Resolution Imaging Spectroradiometer Terra (T), Moderate Resolution Imaging Spectroradiometer Aqua (A), and Visible Infrared Imaging Radiometer Suite (V) Matchups*

| Region<br>name | Number of matchups |         |         | Correlation |      |      | Median bias |        |        | RMSE  |       |       | $f_{EE}$ |      |      | $f_G$ |      |      |
|----------------|--------------------|---------|---------|-------------|------|------|-------------|--------|--------|-------|-------|-------|----------|------|------|-------|------|------|
|                | T                  | A       | V       | T           | A    | V    | T           | A      | V      | T     | A     | V     | T        | A    | V    | T     | A    | V    |
| Global         | 263,384            | 220,037 | 157,821 | 0.80        | 0.81 | 0.82 | −0.001      | 0.001  | 0.005  | 0.12  | 0.12  | 0.12  | 0.78     | 0.79 | 0.80 | 0.44  | 0.46 | 0.48 |
| ENA            | 41,417             | 32,949  | 23,170  | 0.69        | 0.71 | 0.80 | 0.011       | 0.010  | 0.009  | 0.093 | 0.082 | 0.081 | 0.82     | 0.84 | 0.85 | 0.50  | 0.54 | 0.55 |
| WNA            | 38,031             | 31,238  | 24,626  | 0.55        | 0.61 | 0.58 | −0.009      | −0.004 | −0.005 | 0.085 | 0.086 | 0.13  | 0.83     | 0.84 | 0.84 | 0.54  | 0.55 | 0.56 |
| SAM            | 15,753             | 10,432  | 8,712   | 0.76        | 0.73 | 0.61 | −0.005      | −0.005 | −0.006 | 0.092 | 0.098 | 0.075 | 0.85     | 0.86 | 0.82 | 0.56  | 0.58 | 0.56 |
| EUR            | 68,239             | 59,039  | 41,998  | 0.80        | 0.80 | 0.81 | −0.001      | 0.001  | 0.006  | 0.076 | 0.071 | 0.066 | 0.84     | 0.86 | 0.86 | 0.49  | 0.51 | 0.52 |
| OCE            | 10,661             | 8,595   | 4,722   | 0.39        | 0.46 | 0.43 | −0.015      | −0.005 | 0.007  | 0.075 | 0.070 | 0.088 | 0.82     | 0.83 | 0.78 | 0.54  | 0.59 | 0.54 |
| CAS            | 4,828              | 3,944   | 3,288   | 0.80        | 0.84 | 0.89 | −0.003      | −0.008 | −0.016 | 0.14  | 0.15  | 0.14  | 0.72     | 0.75 | 0.82 | 0.36  | 0.38 | 0.46 |
| SAF            | 8,945              | 6,802   | 4,491   | 0.82        | 0.78 | 0.71 | −0.019      | −0.020 | −0.022 | 0.16  | 0.13  | 0.13  | 0.77     | 0.72 | 0.66 | 0.41  | 0.35 | 0.33 |
| IND            | 8,674              | 7,730   | 4,410   | 0.87        | 0.86 | 0.90 | −0.071      | −0.087 | −0.043 | 0.21  | 0.21  | 0.19  | 0.62     | 0.59 | 0.74 | 0.23  | 0.22 | 0.32 |
| NEA            | 13,556             | 12,620  | 10,419  | 0.88        | 0.89 | 0.89 | 0.019       | 0.015  | 0.013  | 0.18  | 0.19  | 0.16  | 0.70     | 0.73 | 0.77 | 0.31  | 0.33 | 0.38 |
| SEA            | 8,026              | 5,962   | 4,611   | 0.85        | 0.84 | 0.85 | 0.003       | 0.001  | 0.039  | 0.20  | 0.20  | 0.24  | 0.64     | 0.63 | 0.58 | 0.26  | 0.26 | 0.25 |
| NAME           | 34,999             | 31,568  | 19,621  | 0.71        | 0.75 | 0.79 | 0.015       | 0.015  | 0.042  | 0.17  | 0.15  | 0.16  | 0.59     | 0.66 | 0.61 | 0.25  | 0.29 | 0.27 |
| BOR            | 10,255             | 9,158   | 7,753   | 0.75        | 0.76 | 0.82 | 0.018       | 0.017  | 0.007  | 0.11  | 0.11  | 0.16  | 0.79     | 0.82 | 0.90 | 0.51  | 0.53 | 0.66 |

*Note.* RMSE = root mean square error; ENA = Eastern North America; WNA = Western North America; SAM = South America; EUR = Europe; OCE = Oceania; CAS = Central Asia; SAF = Southern Africa; IND = Indian subcontinent; NEA = Northeastern Asia; SEA = Southeastern Asia; NAME = North Africa/Middle East; BOR = Boreal.

4. The fraction ( $f_{EE}$ ) of points matching AERONET within the retrieval's expected level of error (EE). The EE is indicated to be a one-standard-deviation confidence interval such that one standard deviation ( $\sim 68\%$ ) of matchups agrees with AERONET within this bound. For DB, the goal (Hsu et al., 2013) was for an EE of  $\pm(0.05 + 20\%)$  relative to AERONET AOD (i.e., a diagnostic, not prognostic, uncertainty estimate). Validation exercises have indicated that in some regions, DB performs somewhat better than this, and as noted previously, the MODIS DB data set also provides prognostic EE estimates for each retrieval (Sayer et al., 2013), also taking into account QA, solar/view geometry, and surface type. Prognostic uncertainty estimated have not yet been developed for VIIRS DB. The diagnostic EE is used to provide a common reference across the MODIS and VIIRS applications of DB.
5. The fraction ( $f_G$ ) of points matching AERONET within the Global Climate Observing System (GCOS) group goal AOD uncertainty for a climate data record, which is the larger of 0.03% or 10% (GCOS, 2011). While a somewhat tighter requirement than can typically be achieved at present, an advantage of this metric is that it is not sensor-specific and so can be used as a benchmark across multiple different data sets, for example, Popp et al. (2016).

### 3.3. Global and Regional Comparison Statistics

Table 1 shows summary statistics (c.f. section 3.2) for the global and regional comparisons between AERONET and the three DB data sets. The main sites within each region (those where at least one of the satellite data sets provides at least 50 matchups) are shown in Figure 2, giving a rough idea of regional assignment, although all sites available were used. Regional assignment is inherently subjective, but the intent is to perform a first-order stratification of the data into regions of distinct aerosol/surface characteristics, and/or those regions commonly analyzed in scientific studies. To aid in more detailed analyses, site-by-site scatter plots are provided individually in supporting information S1.

Although the Spearman correlation and median bias are preferred over Pearson correlation and mean bias for the aforementioned reasons, to aid in comparability with older studies using those metrics, they are also provided within supporting information S1. Additionally, Table 2 provides these metrics globally and regionally (cf. Table 1). Generally, mean and median biases are similar, while Pearson correlation coefficients are larger than Spearman. This is because, as noted, Pearson correlation is more sensitive to out-of-family data such as a rare high-AOD event at a low-AOD site and may therefore overstate the strength of the association for typical conditions (which is partly why Spearman is preferred). Hereafter, mentions of correlation should be taken to refer to Spearman's rank correlation coefficient and bias to median bias.

**Table 2***As Columns of Table 1, Except Showing Pearson Correlation Coefficient and Mean Bias Instead of Spearman Rank Correlation and Median Bias*

| Region<br>name | Pearson correlation |      |      | Mean bias |        |        |
|----------------|---------------------|------|------|-----------|--------|--------|
|                | T                   | A    | V    | T         | A      | V      |
| Global         | 0.89                | 0.90 | 0.89 | −0.001    | 0.001  | 0.005  |
| ENA            | 0.79                | 0.82 | 0.86 | 0.011     | 0.010  | 0.009  |
| WNA            | 0.79                | 0.82 | 0.85 | −0.009    | −0.004 | −0.005 |
| SAM            | 0.94                | 0.94 | 0.87 | −0.005    | −0.005 | −0.006 |
| EUR            | 0.81                | 0.82 | 0.81 | −0.001    | 0.001  | 0.006  |
| OCE            | 0.62                | 0.82 | 0.44 | −0.015    | −0.005 | 0.007  |
| CAS            | 0.89                | 0.88 | 0.91 | −0.003    | −0.008 | −0.016 |
| SAF            | 0.90                | 0.93 | 0.91 | −0.019    | −0.020 | −0.022 |
| IND            | 0.83                | 0.85 | 0.87 | −0.071    | −0.087 | −0.043 |
| NEA            | 0.92                | 0.92 | 0.92 | 0.019     | 0.015  | 0.013  |
| SEA            | 0.87                | 0.86 | 0.86 | 0.003     | 0.001  | 0.039  |
| NAME           | 0.82                | 0.85 | 0.84 | 0.015     | 0.015  | 0.042  |
| BOR            | 0.90                | 0.92 | 0.87 | 0.018     | 0.017  | 0.007  |

*Note.* ENA = Eastern North America; WNA = Western North America; SAM = South America; EUR = Europe; OCE = Oceania; CAS = Central Asia; SAF = Southern Africa; IND = Indian subcontinent; NEA = Northeastern Asia; SEA = Southeastern Asia; NAME = North Africa/Middle East; BOR = Boreal; T = Moderate Resolution Imaging Spectroradiometer Terra; A = Moderate Resolution Imaging Spectroradiometer Aqua; V = Visible Infrared Imaging Radiometer Suite.

Globally, the metrics are very similar between the MODIS Terra, MODIS Aqua, and VIIRS applications of DB. The overall bias is small ( $<0.01$ ), RMSE is 0.12, and the fractions within diagnostic EE of  $\pm(0.05 + 20\%)$  relative to AERONET AOD and within the GCOS goal uncertainty are also close (0.78–0.80 and 0.44–0.48, respectively). The fact that close to 80%, rather than the theoretical 68%, of matchups are within the EE is consistent with prior DB validation studies (Sayer et al., 2013; Sayer, Hsu, Bettenhausen, Jeong, et al., 2012; Sayer, Hsu, Bettenhausen, Jeong, & Meister, 2015; Sayer, Munchak, et al., 2014) which found that global-average performance is somewhat better than this. The total number of matchups reflects the differing lengths of the Terra, Aqua, and S-NPP missions to date. Regional count differences between sensors do not always mirror the global picture because the AERONET network expansion through time has changed the relative geographical distribution somewhat, with coverage expanding proportionately more rapidly in eastern Asia in recent years.

The GCOS compliance fraction is similar between the three data sets (0.44–0.48) but is slightly lower than range of results from three Advanced Along Track Scanning Radiometer (AATSR) AOD retrieval algorithms reported by Popp et al. (2016) of 0.51–0.62 over land. The sample for the AATSR analysis was drawn from only 1 month of data (September 2008), however, and so those numbers might not be representative of broader-scale performance. Popp et al. (2016) included full-mission (2002–2012)  $f_G$  calculations for one of the three AATSR algorithms; going from September 2008 only to the full mission decreased  $f_G$  from 0.62–0.52 for that data set. This suggests that, over land, larger-scale statistics than provided from 1 month of data are necessary to estimate these levels of uncertainty robustly. AATSR made near-simultaneous measurements of the Earth from two view angles (near-nadir and  $\sim 55^\circ$  forward); this dual-view capability is useful for separating atmospheric and surface contributions to the satellite signal, which helps with AOD retrieval over land compared to single-view sensors and may explain the higher  $f_G$  for the AATSR data. The GCOS compliance fraction has not yet been widely adopted in satellite AOD validation exercises, which makes comparative assessment difficult at the present time, so Table 1 provide one benchmark for future global/regional validations with other data sets.

Figure 3 shows the percentiles of AERONET AOD versus those of DB AOD for the three sensors in each region, in spacings of 5% from the 5th–95th percentiles of matched data. This gives an indication of the



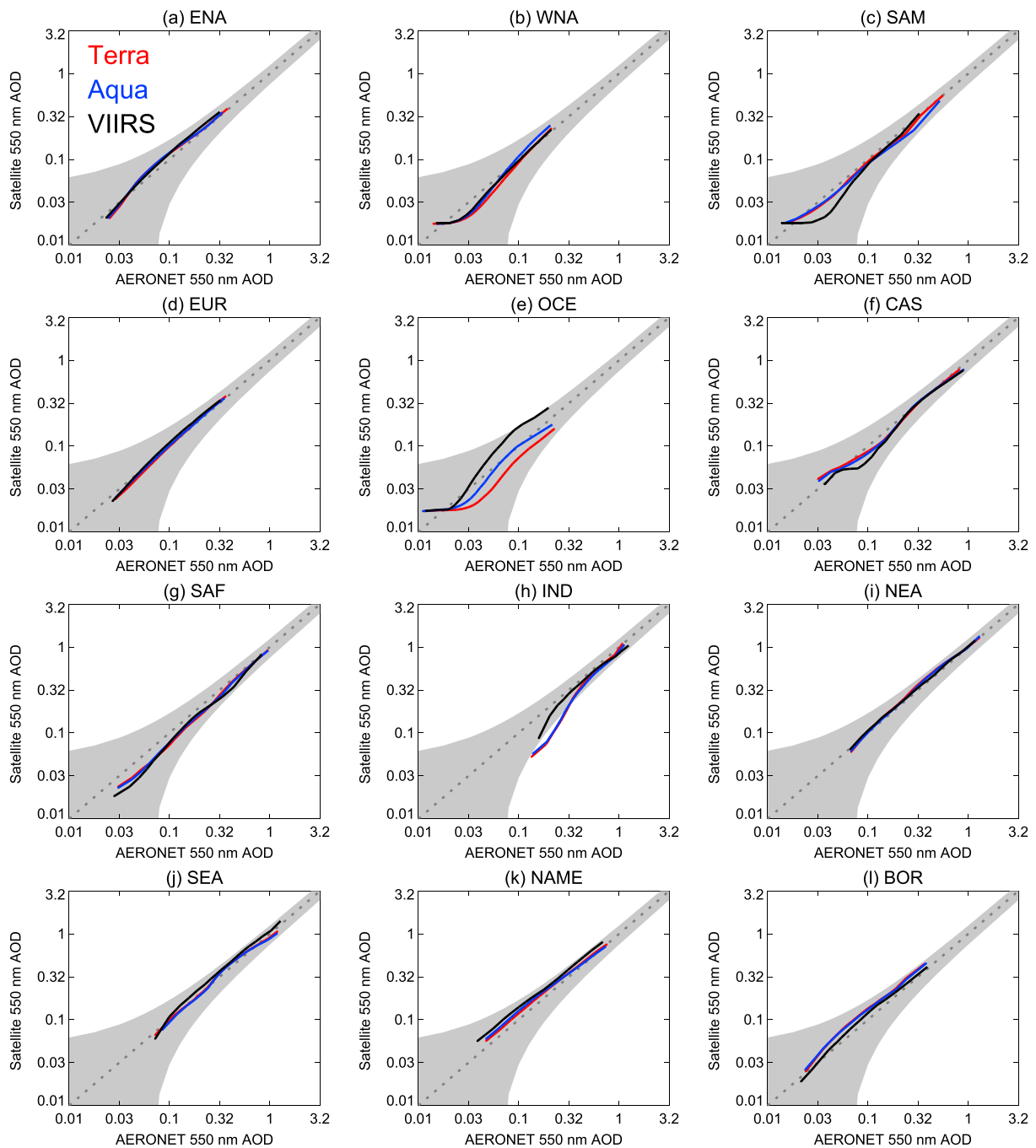


**Figure 3.** Percentiles of AERONET versus MODIS Terra (red), MODIS Aqua (blue), and VIIRS (black) AOD at 550 nm for each region (Figure 2). Data shown for the 5th–95th percentiles of AOD from matchups in each region (a–l). The dashed dark gray line indicates 1:1, and the shaded gray area indicates the EE of  $\pm(0.05 + 20\%)$  relative to AERONET.

distributions and dynamic range of AOD in each region and, in combination with Table 1, provides an overview of the performance of the DB retrievals. These are discussed briefly below, as many applications of DB focus on specific geographic areas. Dubovik et al. (2002) provide some background information on regional variations in aerosol sources, loadings, and optical properties used to describe the below; Reid, Eck, et al. (2005), Reid, Koppmann, et al. (2005), and van der Werf et al. (2010) provide additional context for smoke-dominated regions. Additional references for further information are provided below for some regions. The reader is also directed to supporting information S1 for additional plots and statistics.

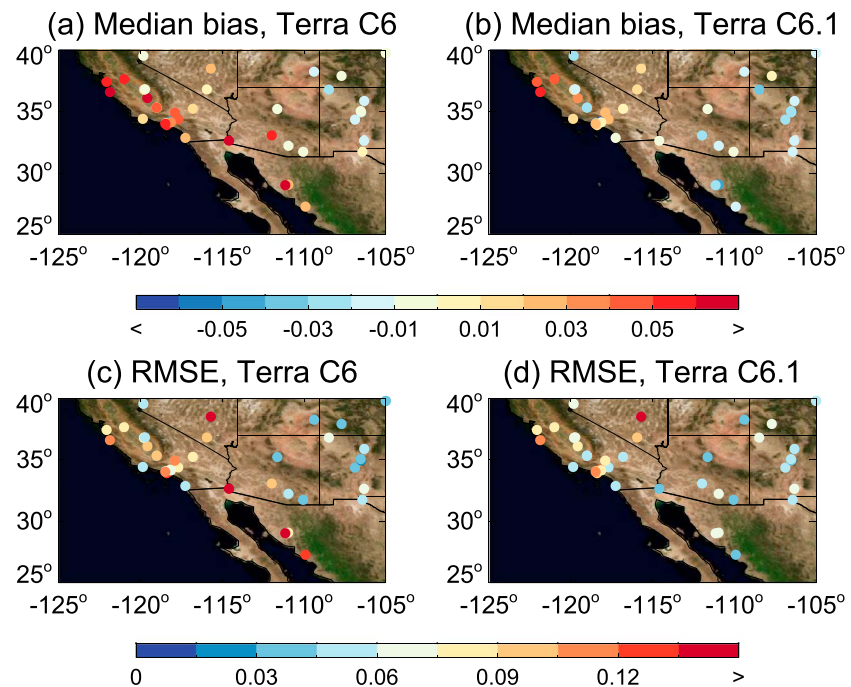


**Figure 4.** Median bias (a, b) and RMSE (c, d) for MODIS Terra DB data from C6 (left) and C6.1 (right) in the semiarid/elevated portion of WNA. Statistics are shown for sites with at least 50 matchups.

### 3.3.1. Eastern North America, Western North America, and Europe

These three regions account for over half of the matchups in each of the data sets. Eastern North America (ENA) is a predominantly low-AOD region (central 90% range of AOD from AERONET and DB is around 0.02–0.3), comprising mainly vegetated and suburban sites across the United States, southern Canada, and around the Gulf of Mexico and Caribbean. These sites typically sample background continental and locally generated aerosols, although can also be influenced by local and transported biomass burning smoke (particularly on the northern end) and mineral dust (particularly on the southern end). Aerosol conditions in Western North America (WNA) are similar to ENA, although the land surfaces tend to be brighter (more arid) and more elevated and more of the cities in this region sit in bowl-like terrain which can cause local buildup of pollution. The drier climate in parts of this region means that smoke is often more absorbing, and dust storms more common, than in ENA (Sayer, Hsu, et al., 2014). All these factors also apply to Europe (EUR).

Comparative statistics in these regions are very similar between MODIS Terra, Aqua, and VIIRS, with a few exceptions. The bulk of the statistics is better than the global average. Correlation is lower than global-average results due to in part the lower dynamic range of AOD compared to elsewhere (with the exception of EUR, due to transported mineral dust and wildfire smoke to some sites). Particularly in WNA, correlation is also depressed by the low range of AOD over clean mountainous sites and by occasional positive outliers at difficult-to-characterize surfaces such as dry lake beds and cities in rugged terrain. In the latter case, these outliers also increase RMSE. Despite these remaining difficulties, Figure 4 illustrates that the situation is improved from C6, with smaller biases and RMSE at many of the sites in the affected part of WNA. Spatial patterns for MODIS Aqua and VIIRS (not shown) are similar. The site with the highest RMSE is Railroad Valley (38.5° N, 115.7° W); this is also the site contributing most to VIIRS having an overall higher RMSE in this region, due to a small number of extreme outliers. This site is located in a dry lake bed which, over retrieval spatial scales, includes steep slopes and areas which can periodically flood (both changing the surface reflectance in unexpected ways which are not captured by the retrieval's surface model).

### 3.3.2. South America

The South America (SAM) region consists of two main types of site: cities (largely coastal), which tend to be low-AOD overall, and sites within or strongly influenced by the Amazon basin. The Amazonian sites have high cloud cover (which limits data coverage) and low AOD in the wet season and large-scale smoke from biomass burning in the dry season, peaking from August–October (Rizzo et al., 2013). During the dry

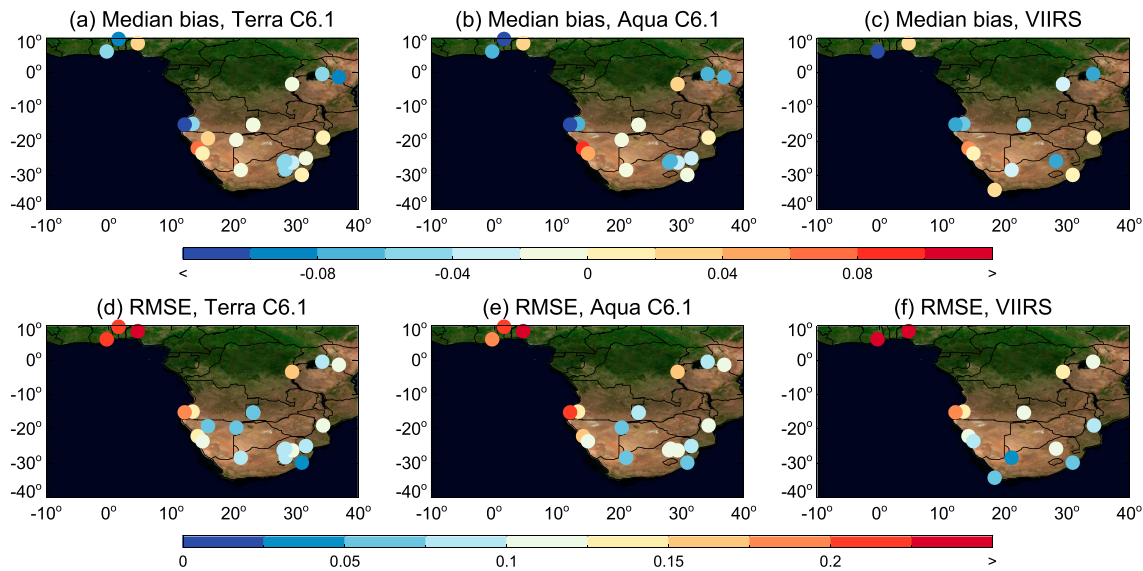


**Figure 5.** Median bias (a–c) and RMSE (d–f) for MODIS Terra C6.1 (left), Aqua C6.1 (middle), and VIIRS v1 (right) in SAF. Statistics are shown for sites with at least 50 matchups.

season, smoke can be transported across the bulk of the continent. Dust transport from the Sahara is also a periodic contribution to aerosol loading in the northern part of this region (Koren et al., 2006).

Performance in SAM is also better than global average, and again, statistics are similar between the three sensors. Going to individual sites (see supporting information S1), the data capture the dynamic range of AOD at sites influenced by biomass burning well. VIIRS has a slightly lower correlation across the region as a whole, because it samples the sites at more southern latitudes (which have a lower AOD and smaller dynamic range overall) comparatively more frequently than MODIS. This is in part because of VIIRS' broad swath meaning these latitudes are viewed more frequently, but also because most of these sites are coastal (which degrades DB retrieval QA), and VIIRS' finer retrieval pixels mean there are valid retrievals within the averaging area more frequently.

### 3.3.3. Oceania

All well-sampled sites in Oceania (OCE) are from Australia. These sites are split between desert regions and cities. These are some of the lowest-AOD regions within the AERONET network, with the lowest fifth percentile of AOD being around 0.01 and the 95th percentile around 0.2. Rare high-AOD events tend to be wildfire smoke and are most concentrated around (but not limited to) sites in northern Australia (Qin & Mitchell, 2009).

Due in large part to the low AOD, correlation for all three sensors is fairly poor (0.39–0.46), but the fraction matching within the EE is high (0.78–0.83). MODIS Terra tends to be  $\sim 0.01$  lower, and VIIRS  $\sim 0.01$  higher, than Aqua; this is reflected in Figure 3. These offsets are consistent with small differences in sensor calibration and/or spectral response functions, as due to the way errors propagate the effects of these factors are amplified in low-AOD, bright-surface conditions. Global patterns of AOD difference will be discussed further in section 4.

### 3.3.4. Central Asia

Central Asia (CAS) is sparsely sampled; the few available sites are largely in mountainous arid terrain. This region includes sites within and downwind of the Taklamakan and Gobi deserts and so the most common departures from clean background conditions are due to local or transported mineral dust (Wang et al., 2017). Most of these sites are within or near cities, with local urban aerosol sources (Abdullaev et al., 2014).

Although this shares some common characteristics with OCE, AOD in CAS is much often higher (Figure 3). Correlation is significantly higher, and there also appears to be less of an offset between the sensors. VIIRS performance is better than the others overall because around a third of the VIIRS matchups are for Dushanbe (38.6° N, 68.9° E) compared to about a tenth for MODIS Terra/Aqua, and performance is overall good and similar at this specific site. The site lies outside the city of Dushanbe, which is in a valley, and a combination

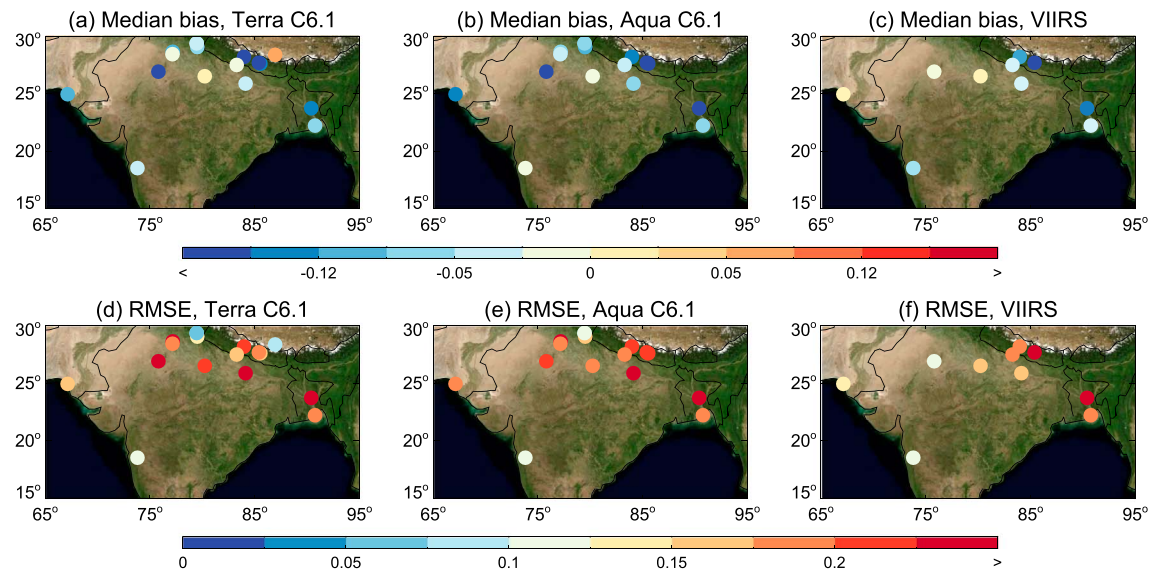


**Figure 6.** As Figure 5, except for sites in IND.

of internal QA tests and elevation gradients means again that the finer spatial resolution of the VIIRS data provide more frequent retrievals. Unfortunately, there are insufficient sites in this region to cancel out the effect of sampling differences at individual sites like this.

### 3.3.5. Southern Africa

Southern Africa samples biomass burning aerosols from various source regions and fuel types at differing parts of the year (Roberts et al., 2009). Eck et al. (2013) also found temporal variation in aerosol single scattering albedo (SSA) within this region. Sites in the northern (Sahelian) part of the region may also, particularly in winter, be influenced by transported Saharan dust (e.g., Pandithurai et al., 2001).

From Table 1 and Figure 3, retrievals here perform slightly poorer than global average, with a consistent tendency for a low bias against AERONET. The data volume for VIIRS is smaller than would be expected given the mission lengths, due to the fact that several key sites (chiefly Djougou, Nairobi, Skukuza, and Wits University) were not in operation for much/any of the VIIRS era. As there is some heterogeneity in performance in this region, this can skew the apparent statistics, and so it is worth examining subregional patterns in more detail. These are shown in Figure 5.

The spatial patterns of bias and RMSE are similar, indicating a general consistency in error characteristics. Sites in the Sahel (Djougou, Ilorin, and Koforidua) have the highest RMSEs, which is in large part, a reflection of the high AOD encountered at these sites, although the fractions matching within the EE are still high (from 61–89% dependent on sensor and site). The reasons for the differing biases between these sites are unknown, given that they experience similar aerosol conditions, and are in similar terrain (flat, semi-arid, near but not within cities). To the east and slightly south, Bujumbura, Nairobi, and ICIPE Mbita (the former two cities, the latter on the edge of Lake Victoria) have lower RMSE and smaller biases, with Bujumbura the most positive biases/largest RMSE of the trio. All three sample biomass burning aerosols during certain seasons and the two city sites may also have local sources. These sites are in elevated terrain, which has been seen in prior DB data versions to be linked to low biases (Sayer et al., 2013) due to approximations made about vertical structure in the retrieval forward model. Similar reasoning explains the behavior of the bulk of sites further south in this region, which are also typically elevated, in urban or semiarid areas, and sample seasonal biomass-burning aerosols. Sites in Namibia and Angola along the western coast of Africa have larger RMSE. Namibe (15.2° S, 12.2° E) is on a river mouth, subject to rapid changes in surface reflection following rainfall. Henties Bay (22.1° S, 14.3° E) is also coastal and around a desert. From time to time, small convective cumulus clouds form along the coastline; examination of a few scenes (not shown) finds that these are sometimes missed by the cloud mask.

### 3.3.6. Indian Subcontinent

The aerosol system for the various countries and ecosystems included in the Indian Subcontinent (IND) is highly complex and has been the focus of much study for decades (e.g., Dey & Di Girolamo, 2011;



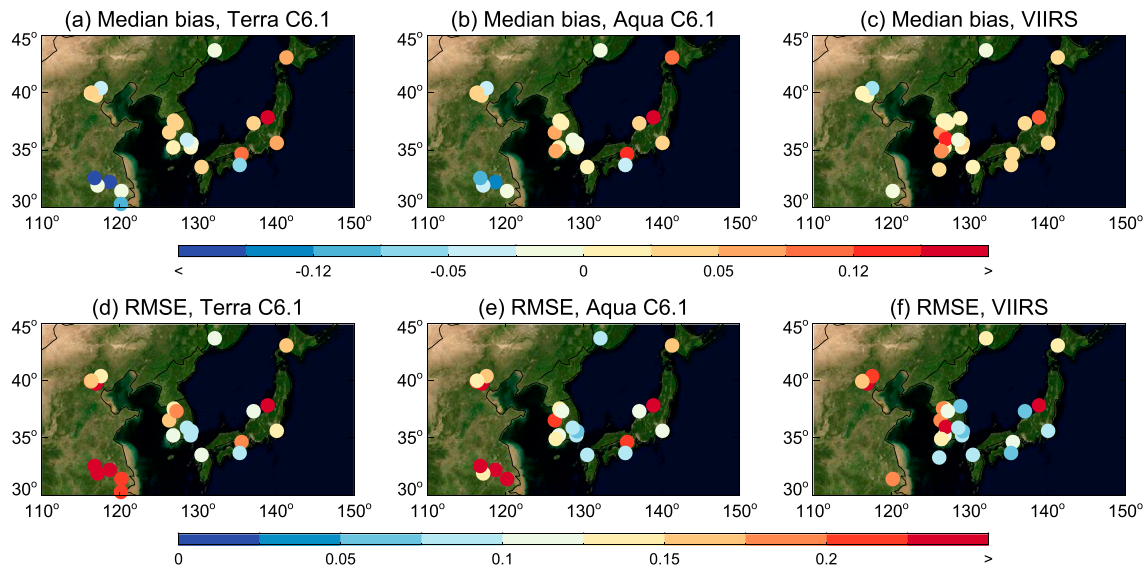


**Figure 7.** As Figure 5, except for sites in NEA.

Gautam et al., 2011; Henriksson et al., 2011; Negi et al., 1967; Parekh et al., 1967; Sharma et al., 2012). The bulk of the AERONET sites available is in or near the Indo-Gangetic Plain (IGP), in Pakistan, India, Nepal, and Bangladesh, and is subject to seasonally and spatially varying contributions from mineral dust, smoke, and urban/industrial aerosol sources. The monsoon season is also a strong limit on coverage (for both satellites and AERONET data) from June–October.

Bias and RMSE for sites in IND are shown in Figure 6. All three sensors underestimate AOD in this region, leading to higher RMSE and lower fraction within EE than in other regions; VIIRS performs somewhat better than either MODIS sensor (Table 1). This is due to adjustments to surface and aerosol models in this region which were initially tested with VIIRS and were not implemented in MODIS C6.1 due to a lack of time before the deadlines for the MODIS C6.1 data reprocessing. This inconsistency will be rectified at the next opportunity for a MODIS reprocessing. These updates have decreased the magnitude of bias and RMSE at many sites across the IGP. However, the overall tendency for a low offset versus AERONET remains. In particular, performance at sites in Nepal and Bangladesh did not change. VIIRS has fewer sites available, as several ceased operation prior to the VIIRS launch. The single site with a large positive bias in MODIS Terra is in rugged terrain in the Tibetan Plateau; this has fewer than 50 matchups with Aqua (but a similar pattern for those matchups), and none with VIIRS, although the site is still operating.

### 3.3.7. Northeastern Asia

Most sites in Northeastern Asia are in dense urban areas in eastern China, Korea, and Japan. Some are in mountainous terrain, which may be above low-level aerosol layers. Generally, these sites are influenced by local urban/industrial sources, as well as (singly or combined) transported industrial, dust, and periodic wildfire smoke (Henriksson et al., 2011; Hsu et al., 2006; Park et al., 2007). These factors combine to provide AOD minima and maxima which are larger than that of most other regions (Figure 3).

Correlation and fraction within EE in this region remain high, although RMSE is also larger than global average due to the high AOD, and performance is broadly consistent between sensors (Figure 7). In brief, biases tend to be positive over much of the region, aside from several sites around Shanghai where it is negative. The aforementioned various sources contributing to periodic aerosol transport mean that the aerosol composition is complicated and can vary rapidly with time. It is likely that substantial reduction of these biases (and so RMSE) will require more robust identification of aerosol type and selection of aerosol optical models. Recently, Sogacheva et al. (2018) validated MODIS Terra C6.1 data in China, covering many of these sites, and provided discussion about performance in various subregions. These results are broadly consistent with that analysis, although the validation methodology was slightly different.

### 3.3.8. Southeastern Asia

Southeastern Asia also has a large number of sites in challenging coastal and urban areas. These sites can be strongly influenced by seasonally varying biomass burning smoke from crop fires (particularly from



Myanmar and Thailand in February–April; Gautam et al., 2013) and peat fires from Indonesia later in the year (Salinas et al., 2013). The strength of these fires is influenced by El Niño; 2006 and 2015 had particularly strong smoke as a result (Field et al., 2016). High cloud cover, particularly of optically thin cirrus, is a perpetual challenge to AOD retrieval and quality from both ground-based and spaceborne platforms here (Chew et al., 2011; Huang et al., 2011; McFarquhar et al., 2000; Reid et al., 2013)

Due to these coverage limitations and a small number of sites, the data volume in Southeastern Asia is low. Despite this, the correlation is high overall, indicating that the retrieval is able to identify some of the smoke-dominated scenes without suffering significant false positives from cloud contamination. Many of the sites available in this region are fairly new, and a more detailed analysis of subregional performance is likely to require additional years of data, particularly for those sites in Indonesia. The sites in Thailand and Vietnam provide the bulk of the data here. The overall near-zero bias masks negative and positive biases in high-AOD cases at individual sites; these in part appear to be linked to elevation, with negative biases seen at higher-elevation sites, consistent with other regions.

### 3.3.9. North Africa/Middle East

Most sites here sample dust from the Sahara or Arabian Peninsula, at various distances from source regions. This region is the largest global source of mineral dust aerosol, which is often transported out of the region, and intense dust storms can produce very high AOD (Ginoux et al., 2012; Prospero et al., 2014; Ridley et al., 2016). Sites around the coast tend to be cities, which show fairly low AOD outside dust episodes. Sahelian sites also sample urban aerosols and, particularly in the winter, biomass burning smoke mixed with dust (Rahot, 2008). Like IND, some aerosol and surface model improvements were made to the VIIRS DB code in this region but could not be implemented in the MODIS code before the C6.1 reprocessing, leading to potential regional offsets. These differences do not affect the AERONET comparison very much (Table 1), and neither MODIS nor VIIRS are better across all statistics for this region. The larger-scale effects of these algorithm differences will be examined in Figure 4. This region contributes the most to the dust-dominated bright-surface scenes analyzed in section 3.6, and general comments made later there apply to many of the sites in this region.

### 3.3.10. Boreal

The Boreal (BOR) region is a catch-all for sites at high Northern latitudes, mostly in low-AOD cities or rural areas. In summertime, wildfires from forest and/or peat burning (Chubarova et al., 2011; Turquety et al., 2007) can lead to widespread (sometimes transported around the hemisphere; Damoah et al., 2004) smoke. Likewise, a common challenge for sites in these regions is retrieval availability and quality in winter months, due to a combination of cloud and snow cover with low Sun angles and polar night.

Performance in BOR is again fairly similar to that in ENA and EUR, likely due to (outside the northern limit) similar surface and aerosol conditions. Smoke from fires in this region tends to be weakly absorbing (midvisible SSA from 0.95–0.99) as it is frequently smoldering combustion of peat fires, or if it does start with lower SSA often becomes less absorbing as it ages (Chubarova et al., 2011; Eck et al., 2003, 2009). The DB algorithm makes similar SSA assumptions, and as a result, biases in the retrieval are fairly small in smoke-dominated conditions at sites in BOR. VIIRS has a higher RMSE due to a small number of outliers in high-AOD conditions; manual inspection of a few dates suggest that MODIS does not provide a retrieval during some of these cases. Other than that, VIIRS performance is slightly better than that of MODIS. The high latitude means that VIIRS sees many of these sites twice or more per day, leading to a greater data volume than would be expected from mission length.

## 3.4. MODIS Terra Versus Aqua

The previous sections have hinted that, as expected, the overall performance of DB applied to MODIS Terra and Aqua is similar. This section provides a more direct comparison between validation summary statistics between the two sensors. Figure 8 compares site-by-site validation metrics for the two MODIS sensors; this is restricted (aside from the data count comparison) to the 436 sites where both Terra and Aqua provide at least 50 matchups with AERONET. Further, Table 3 provides statistical metrics for each of the panels in Figure 8. These reveal that, indeed, MODIS DB Terra and Aqua data have similar performance at the level of individual sites. The correlations between metrics for Terra and Aqua are high (between 0.89 and 0.97). Looking at the median (Terra–Aqua) differences in statistics, Aqua tends to perform slightly better overall (RMSE lower by 0.005 and 1.5% more matchups agreeing within EE). This is not unexpected, given the greater calibration degradation of the Terra sensor and associated difficulties. Terra does tend to have more retrievals than Aqua. In part, this is due to the earlier mission launches (2000 vs. 2002), but as only a small

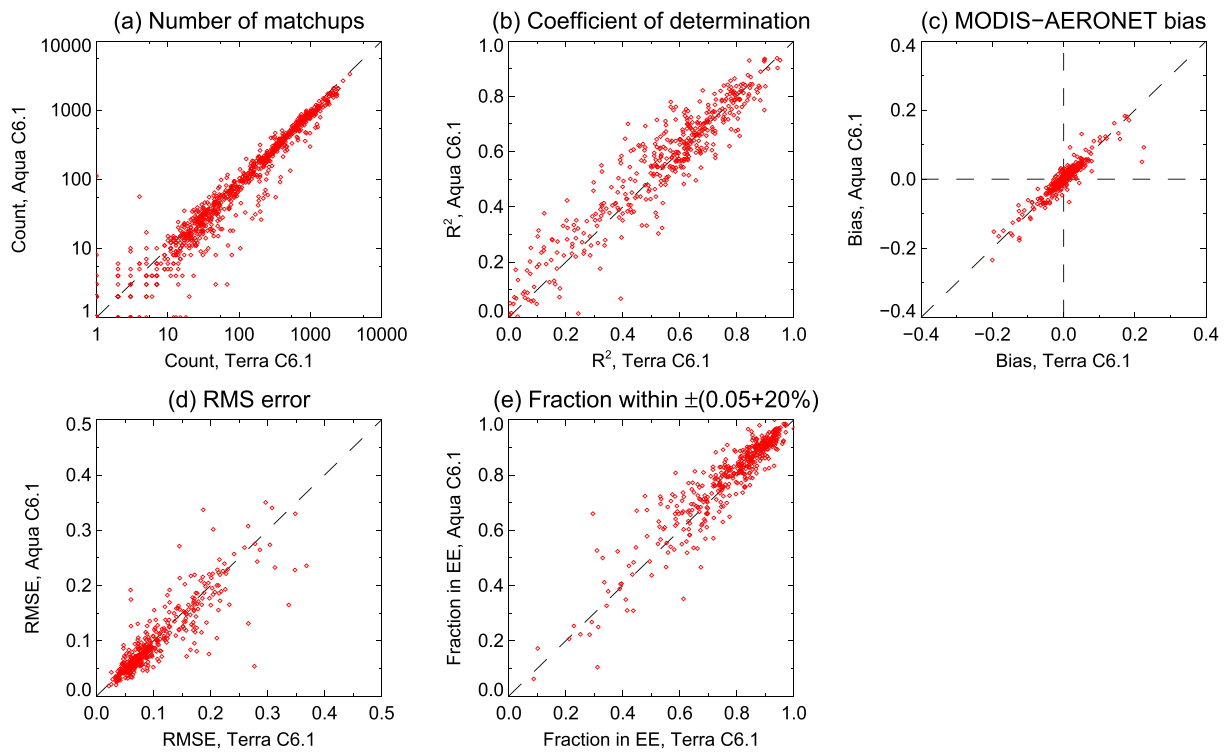


**Figure 8.** Comparison of site-by-site validation statistics (a–e) for MODIS Terra versus Aqua DB C6.1 AOD data. For (b)–(e), points are only shown where both sensors provide at least 50 matchups.

number of AERONET sites were in operation for the period 2000–2002, it is likely that this is dominated by retrieval availability differences due to cloud cover, which show diurnal behavior dependent on cloud type (e.g., Eastman & Warren, 2014). Terra sampling is influenced more by early morning fog (which in many cases may have burned off by the 10:30 overpass time), while Aqua is influenced more by daytime convection.

Despite the overall similarity, there are a few outliers. The site with the largest difference in RMSE is the Swedish Meteorological and Hydrological Institute (SMHI) (58.6° N, 16.2° E), where Terra has a RMSE of 0.28 and Aqua 0.05. This turns out to be due to one outlying matchup in the Terra data where DB retrieved an AOD of 3.5 in low-AOD conditions; other than this one point, the Terra and Aqua matchups are very similar. Thus, the difference in the site summary statistic corresponds to a single outlier in the Terra data. The site with the next-largest difference in RMSE is Mussafa (24.4° N, 54.5° E), which has an RMSE of 0.34 for Terra and 0.17 for Aqua. This site also has the largest difference in  $f_{EE}$ , 0.30 for Terra versus 0.66 for Aqua. This is a particularly complex site: within the city of Abu Dhabi, which is also coastal and on a desert.

**Table 3**

*Correlation, Median (Terra–Aqua) Difference, and Standard Deviation of Difference in Moderate Resolution Imaging Spectroradiometer Terra/Aqua Deep Blue Collection 6.1 Site-by-Site Validation Statistics Shown in Figure 8*

| Metric                         | Correlation | Median difference | Standard deviation of difference |
|--------------------------------|-------------|-------------------|----------------------------------|
| $\log_{10}$ number of matchups | 0.97        | 0.060             | 0.12                             |
| $R^2$                          | 0.91        | −0.012            | 0.079                            |
| Median bias                    | 0.91        | −0.0002           | 0.018                            |
| RMSE                           | 0.89        | 0.005             | 0.031                            |
| Fraction in EE                 | 0.93        | −0.015            | 0.062                            |

*Note.* RMSE = root mean square error; EE = expected level of error.

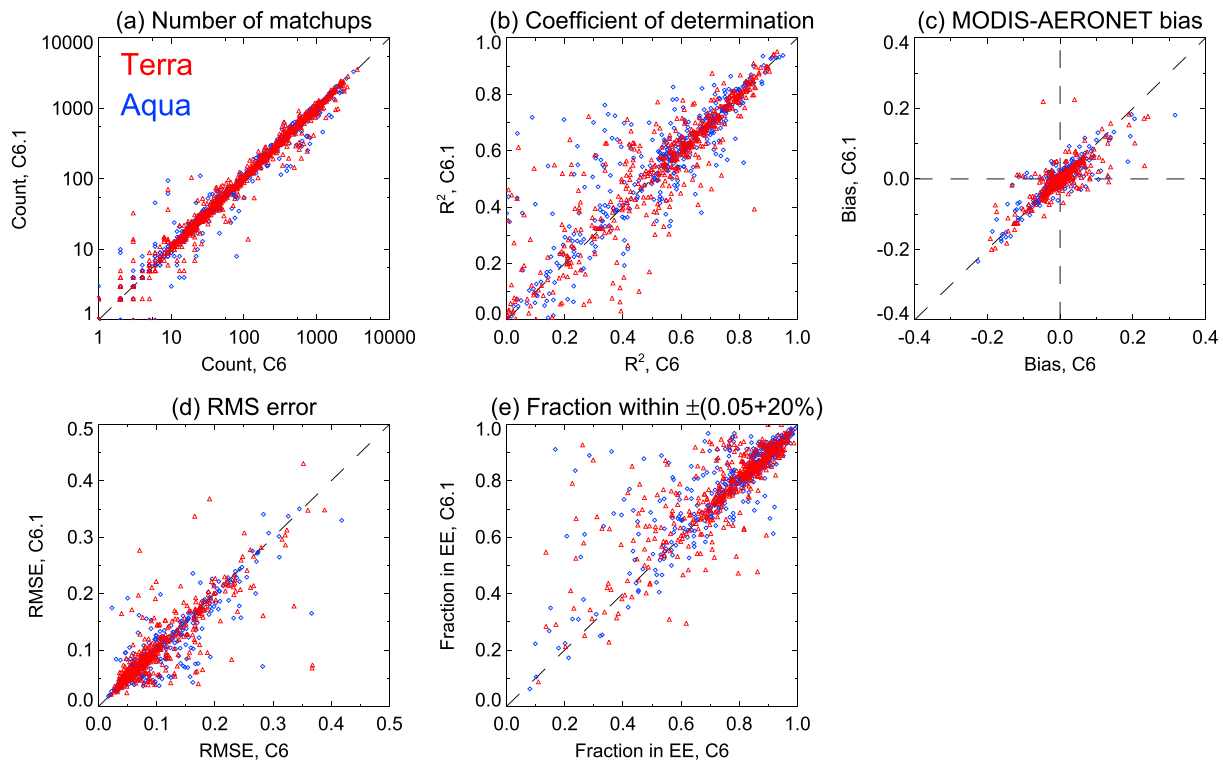


**Figure 9.** As Figure 8, except comparing MODIS DB results for C6 and C6.1, for Terra (red) and Aqua (blue) data separately.

Both Terra and Aqua retrievals at this site (cf. supporting information S1) show two distinct groupings of retrievals: one performing well and the other poorly (biased high). The Terra matchups draw more strongly from this latter population. This is likely due to inadequacies in the surface reflectance model used in this highly complex terrain at certain geometries, which may be encountered more frequently by Terra than Aqua. In both sensors, these high-biased points can occur year-round; as this site is in the tropics, there is less variation in scattering angle than for higher-latitude sites. Several of the other sites with larger Terra-Aqua differences in performance (e.g., Al Khaznah, Masdar Institute) are also in this area and so likely suffer from the same difficulties.

### 3.5. MODIS C6 Versus C6.1

Another relevant question to ask is to what extent MODIS C6.1 represents an improvement on the previous C6. Figure 9 is analogous to Figure 8, except comparing C6 versus C6.1 validation results. This is drawn from the 459 (Terra) and 431 (Aqua) sites with at least 50 matches with AERONET in both collections. In general, points still lie close to the 1:1 line, indicating that on a large scale, the performance of C6 and C6.1 shows similar general tendencies. Taking a closer look, Figure 10 shows histograms of the difference between the two collections and also indicates the fraction of sites where C6.1 is better (i.e., higher data volume, higher  $R^2$ , smaller bias, smaller RMSE, and higher  $f_{EE}$ ) than C6. For every metric but one, for both Terra and Aqua, a majority (51.0–59.7% of sites) perform better for C6.1 than C6. The exception is RMSE for Terra, for which the difference between collections is negligible (49.9% better in C6.1). All these distributions peak near zero, although the tails of the distributions are wider on the side of improvement. This indicates that while overall, the improvement is slight, at certain sites, it is significant (these sites being the outliers in Figure 9), and there are fewer cases of large degradations in performance than large improvement. Small apparent positive or negative changes in statistics are the result of small systematic changes (e.g., calibration) as well as statistical noise in the metric due to limited sampling.

The sites with the largest overall improvement (in terms of smaller RMSE and/or higher  $f_{EE}$  in C6.1) include several which have been highlighted earlier in this study. For both Terra and Aqua, these include sites in rugged terrain and/or near salt pans, such as the sites in WNA shown in Figure 4, coastal Southern Africa in

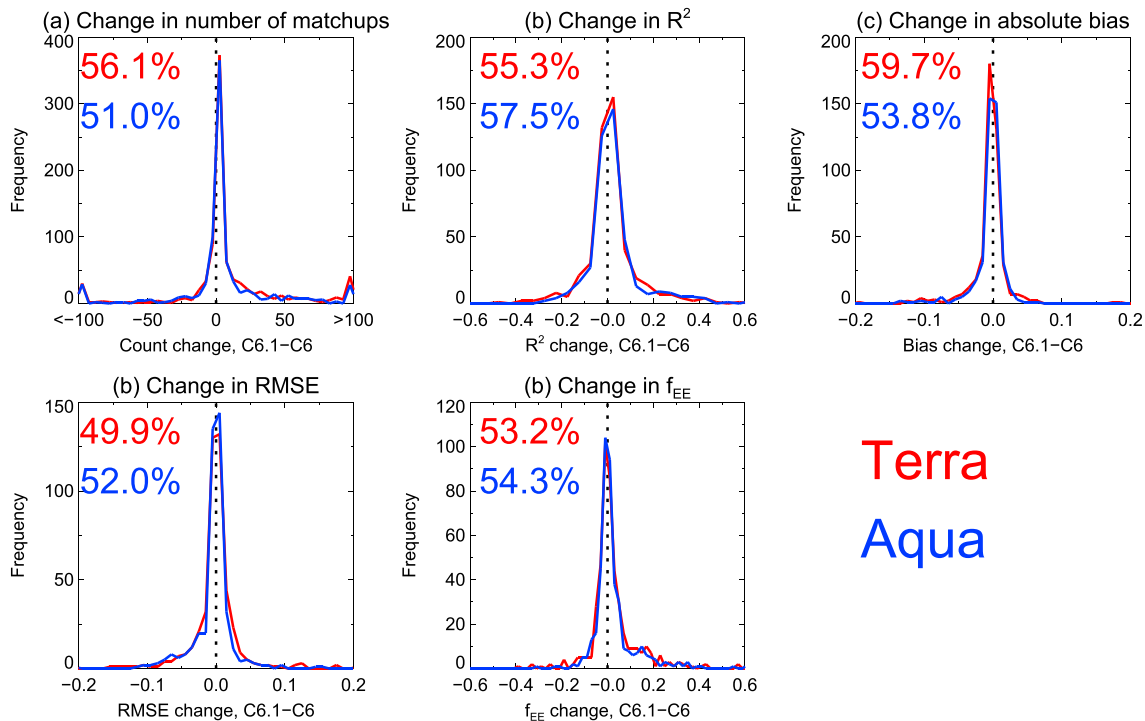


**Figure 10.** Histograms of the site-by-site validation metrics shown in Figure 9. Numbers indicate the fraction of sites for which C6.1 is better. Data and figures shown for Terra (red) and Aqua (blue) data separately.

Figure 5, and sites in valleys like Dushanbe. These sites benefited from efforts to improve surface reflectance models and QA tests in these terrain types; these algorithm updates will be described in a forthcoming paper.

On the other side, several sites do show a nonnegligible increase in RMSE and/or decrease in  $f_{EE}$  going from C6–C6.1. Examining the largest of these, several (e.g., SMHI, discussed previously) result from attempts to increase spatial coverage (which were successful, increasing data volume by 10–20%) with the downside of rare additional cloud/snow contamination. These sites tend to be at high northern latitudes, where this is a particular difficulty in winter, and for Terra, due to the lower Sun during the time of the satellite overpass. The others tend to be clustered around the northern Arabian Peninsula (e.g., aforementioned Mussafa, Masdar Institute sites). In this case it appears that algorithm/calibration changes have had the unforeseen consequence of removing predominantly low-AOD matchups (which tend to have lower RMSE) and slightly increasing the bias of remaining points.

### 3.6. Dependence on Aerosol Loading and Type

It is also useful to examine how the retrieval errors depend on aerosol loading and type. This is addressed in Figure 11, which stratifies the available data into three broad categories based on the AERONET AOD and AE: “background” conditions, defined as  $AOD \leq 0.2$ ; “dust-dominated” conditions, defined as  $AOD > 0.2$ ,  $AE \leq 1$ ; or “fine-dominated” conditions, defined as  $AOD > 0.2$ ,  $AE > 1$ . Figure 11 shows median and variability of retrieval errors as a function of AOD, splitting the points within each category into 10 (for background) and 20 (for the two high-AOD groups) bins. This is further split dependent on whether the retrieval in question was processed with the data base or vegetated surface reflectance paths (Hsu et al., 2013), as these are also expected to show different error characteristics. Note that retrievals from the “mixed” category (cf. Figure 1), when both methods contribute, are grouped here with the vegetated path. This is because they are comparatively few in number and from past experience tend to show similar error characteristics to vegetated retrievals.

It is reassuring (given sensor and algorithm similarities) that in general, the error characteristics are similar between the three sensors. For the background subset, in all cases, the bias is small, and the distribution of retrieval errors is within the expected  $\pm(0.05 + 20\%)$ . For the fine-mode dominated subset, there is a tendency for low bias of order 5–10% over bright surfaces but more like 10–15% over vegetated surfaces.

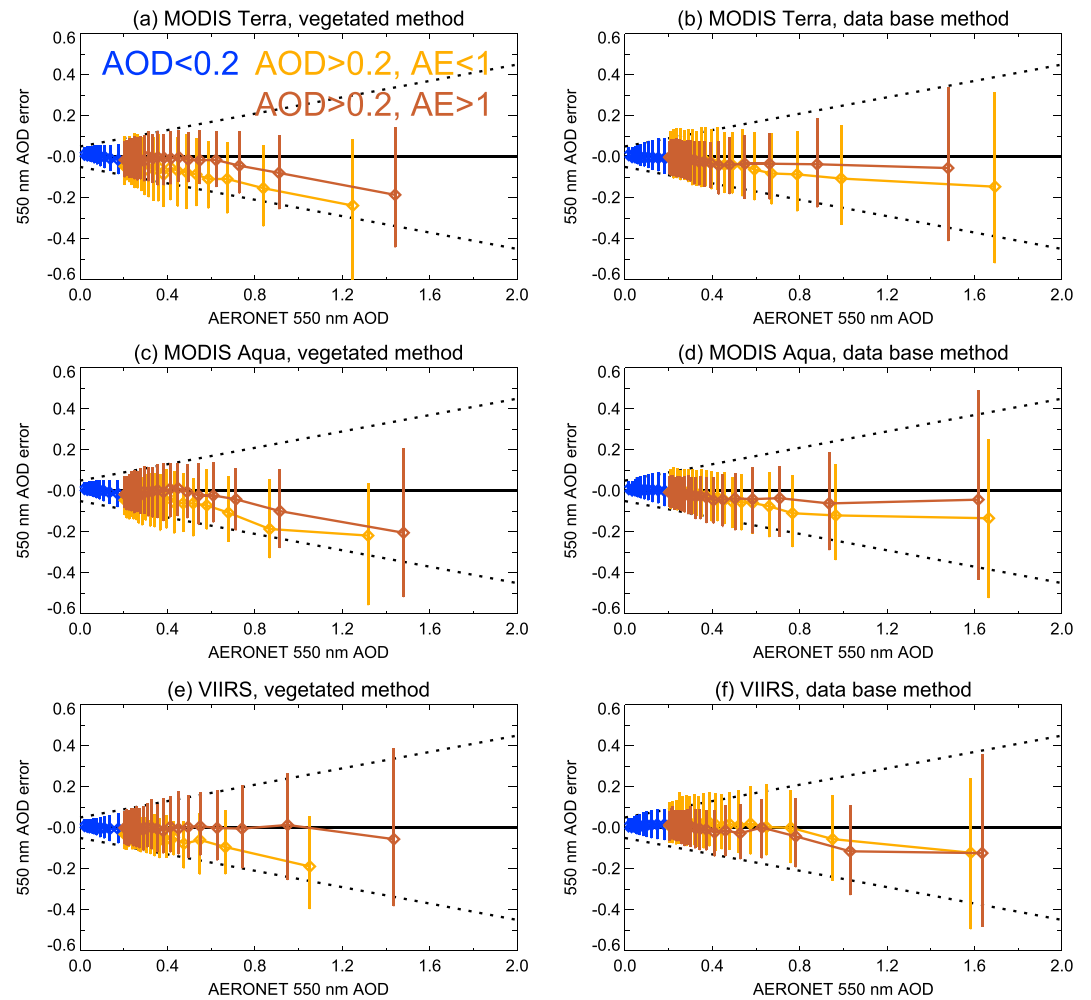


**Figure 11.** Median (points) and central one standard deviation (vertical lines) error in retrieved AOD as a function of AOD, split into background (blue), dust-dominated (orange), and fine-mode dominated (brown) AERONET subcategories and binned (see text). Data shown separately for (a,b) MODIS Terra, (c, d) MODIS Aqua, and (e, f) VIIRS, for retrievals processed with the (left) vegetated and (right) surface reflectance data base retrieval paths. Dashed envelopes indicate the AOD EE:  $\pm(0.05 + 20\%)$ .

In this latter case the bias for VIIRS is negligible, likely due in part to aforementioned algorithm updates implemented over much of India in VIIRS but not yet in MODIS. For the dust-dominated subsets, however, the biases tend to be larger and more negative: 10% over bright surfaces and 15–20% over vegetated surfaces and reasonably consistent between MODIS and VIIRS. In both of these cases, there is a tendency for the retrieved AOD to fall below the EE envelope when the true AOD is approximately 1 or higher. Aside from the general underestimate in AOD, the width of observed errors is comparable to the width of the EE. The top bins, beyond which there is insufficient data volume to robustly assess behavior, are typically for an AOD around 1.6. In these extreme cases, it is likely that aerosol plume spatiotemporal variability may also be larger, which would add further uncertainty to the interpretation.

Figure 12 is equivalent to Figure 11, except for AE. This also reveals very comparable behavior between the sensors but systematic differences based on aerosol loading, aerosol type, and surface type. For the background subsets of data, it appears that in all cases, the width of the AE error distribution is about 0.5, although part of this comes from the nonnegligible uncertainty on AERONET AE in low-AOD conditions (Wagner & Silva, 2008). Note that when DB retrieves an AOD at 470 nm less than 0.2, the AE is not retrieved but instead prescribed with a regionally dependent value.

When AOD is higher, the AE retrieval tends to have a positive bias around 0.2 compared to AERONET, but the scatter shrinks with increasing AOD to around  $\pm 0.25$  in AE. Dust AE is fairly systematically overesti-



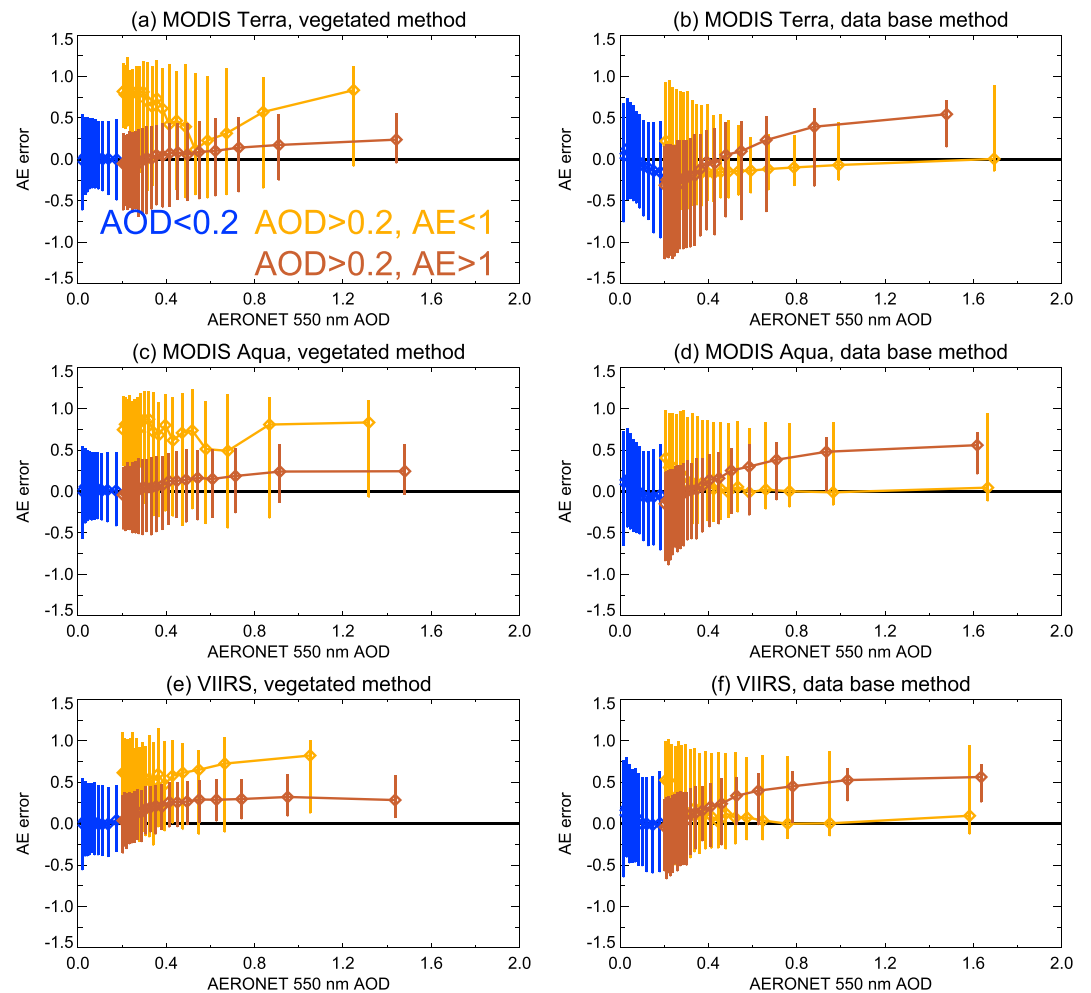


**Figure 12.** As Figure 11, except for AE. Note that the AE has no defined EE.

ated by 0.5–1, with a broad range of error. This suggests that a nonnegligible amount of the time, in dusty cases over vegetated surfaces, the algorithm fails to retrieve a dust-like AE. Improved dust/nondust discrimination would be important to improve AE retrieval over vegetated surfaces. DB includes tests to attempt to identify dust versus smoke (Hsu et al., 2013), although one of the key tests for dust identification is based on thermal contrast and is not robust when column water vapor is high, which is more common over vegetated surfaces than over bright desert or mountain surfaces.

For cases from the data base method for estimating surface reflectance, dust/smoke discrimination is somewhat improved in that the AE bias in dust-dominated conditions is much smaller. These dust-dominated retrievals are mainly drawn from bright desert surfaces in the Sahara desert and Arabian Peninsula. The error distributions remain broad, indicating that while reduced, the misclassification problem remains to an extent. For fine-mode dominated conditions, the uncertainty tends to decrease when AOD is above around 0.4, and the typical offset versus AERONET is larger than over vegetated surfaces. Together, these results suggest that the DB AE should be used only in a qualitative manner to discriminate between fine-mode and coarse-mode optically dominated aerosol columns and that extra caution is needed for identifying dust above vegetated surfaces.

### 3.7. Time Series Stability

AERONET data are a valuable tool to assess the stability of satellite AOD data sets, due to their low uncertainty and regular pre- and post-deployment recalibration. Knowledge of data stability and characterization of any drifts is important for trend analyses; the GCOS goal for AOD stability is 0.01 per decade (GCOS, 2011). Figure 13 shows time series of AOD and AE bias and RMSE against AERONET, for all three sensors,

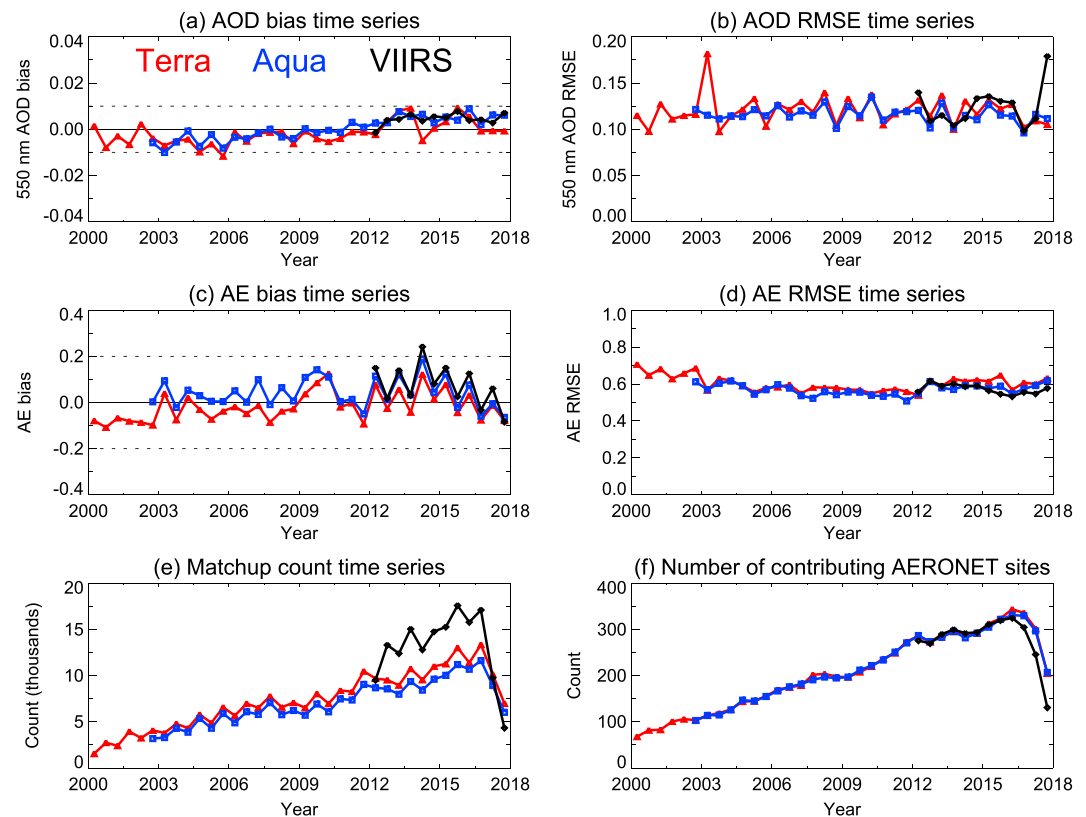


**Figure 13.** Time series of (a, c) bias and (b, d) RMSE for 550-nm AOD and AE, along with (e, f) numbers of contributing matchups and sites, for the comparisons between MODIS Terra (red), MODIS Aqua (blue), and VIIRS (black) DB data with AERONET. Data shown in 6-month increments, for periods with at least 1,000 satellite-AERONET matchups.

split into 6-month periods. With the exception of two coincidental blips in the AOD RMSE (due to a small number of extreme outliers rather than a broader change in the behavior), the time series are fairly smooth. The bias time series show 6-month oscillations, which is due to the uneven distribution of AERONET sites (i.e., predominantly at Northern Hemisphere midlatitudes) and resulting influence of different seasonality of aerosol conditions and data sampling/availability on the matchups. The data also reveal a possible upward trend in the biases over time, which remains generally within  $\pm 0.01$  over the 2000–2017 period. However, this may well be influenced by the large expansion of AERONET, meaning there are around a factor of six more sites and matchups in recent years compared to the early 2000s. Note that the year 2017 shows a decrease in the number of matchups because, at the time of writing, much of the AERONET data collected during 2017 have not yet been raised to L2.

To decrease the potential contribution of changes in the AERONET network to the apparent drifts, Figure 14 repeats the analysis using only the 50 sites missing matchups from no more than six 6-month periods (3 years) from the time series. Sampling remains slightly poorer for 2000–2003 and 2017, but the overall picture looks similar. This implies that the positive AOD drifts may be real.

Table 4 shows the gradients (and one standard deviation,  $1\sigma$  uncertainties) of linear least-squares regression fits to the AOD bias time series shown in Figures 13 and 14. The best estimates of the drift, expressed in AOD per decade are 0.005–0.006 for MODIS Terra and VIIRS and 0.01 for MODIS Aqua and consistent for both the ensemble of AERONET sites as a whole and the more restrictive long-term set. This indicates that DB approximately meets (for Aqua) or exceeds (for Terra and VIIRS) the GCOS stability goal. Aside from VIIRS, where the time series is considerably shorter, the uncertainties on the drift estimates are small, implying confidence in this assertion. The uncertainty calculation assesses and corrects for a one-period (i.e. 6-month) lag autocorrelation, following Weatherhead et al. (1998), reflecting the fact that successive periods may not be fully independent.

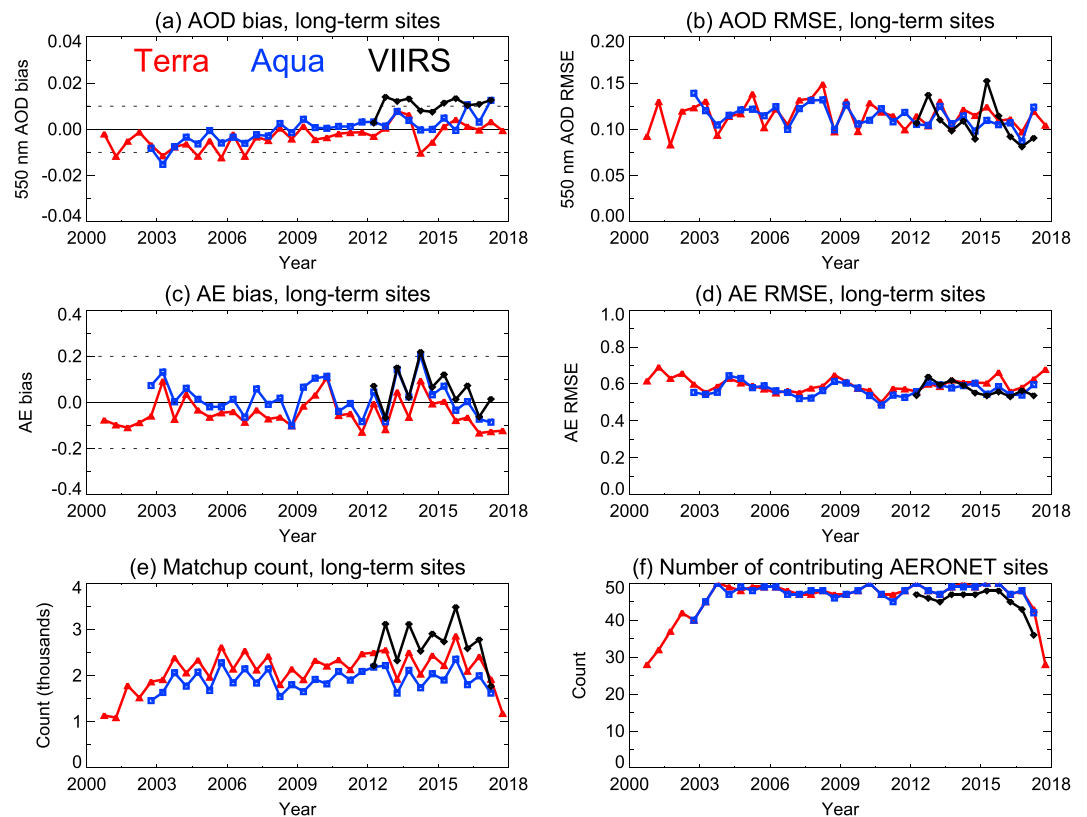


**Figure 14.** As Figure 13, except for only the 50 long-term AERONET sites.

## 4. Global and Regional Patterns

This section investigates various aspects of the consistency between the three DB data sets, using the L3 (D3/M3) data as a basis. Section 4.1 compares the frequency with which the data sets provide retrievals and section 4.2 the consistency of daily-averaged data using common days. Both of these use D3 products from the years 2013–2015 as a basis. Finally, section 4.3 examines regional time series, using M3 products from March 2000 (as only 6 days of MODIS Terra data are available for February 2000) to the latest available at the time of writing.

### 4.1. Patterns of Data Coverage

Figure 15 shows the fraction of days within the 2013–2015 period where each data set provides valid L3 daily data (referred to as “retrieval fraction”). These D3 data products used all require at least three L2 retrievals passing QA checks for a D3 grid cell to be valid. The data are split into two 6-month periods: boreal winter/spring (December–May) and boreal summer/autumn (June–November). Seasonality in coverage is expected due to seasonality in cloud and snow cover and polar night. At a first look, the spatial patterns are

**Table 4**

*Drifts (and  $1\sigma$  Uncertainties) in the Deep Blue Data Sets, Expressed in Units of Aerosol Optical Depth per Decade, Based on the Comparisons at All Sites and Long-Term Sites Only*

| Sensor      | All sites             | Long-term sites       |
|-------------|-----------------------|-----------------------|
| MODIS Terra | 0.005 ( $\pm 0.002$ ) | 0.006 ( $\pm 0.002$ ) |
| MODIS Aqua  | 0.010 ( $\pm 0.002$ ) | 0.010 ( $\pm 0.003$ ) |
| VIIRS S-NPP | 0.006 ( $\pm 0.004$ ) | 0.006 ( $\pm 0.005$ ) |

*Note.* MODIS = Moderate Resolution Imaging Spectroradiometer; VIIRS = Visible Infrared Imaging Radiometer Suite; S-NPP = Suomi-National Polar-orbiting Partnership.

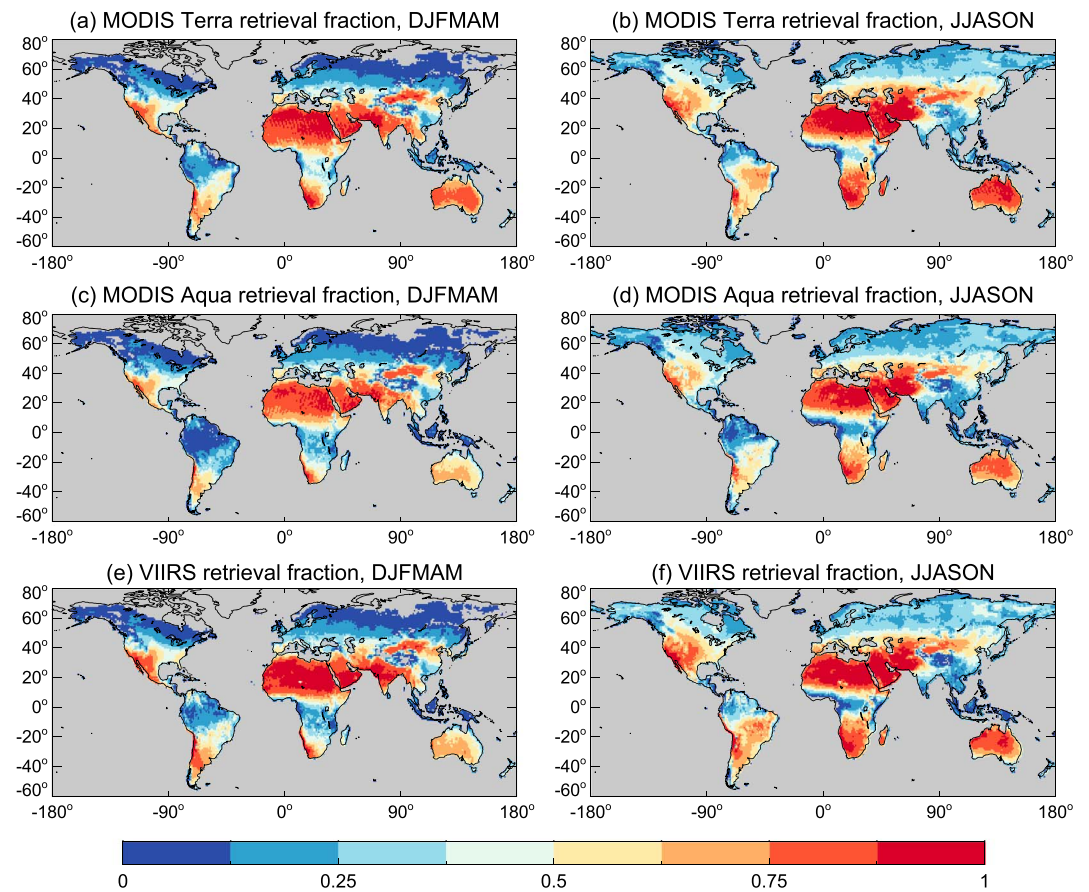


**Figure 15.** Fraction of days with L3 coverage for each data set, for (a, c, e) boreal winter/spring and (b, d, f) boreal summer/autumn. Grid cells with zero valid days are shaded in gray.

(as expected) similar between the three sensors. MODIS Aqua and VIIRS are expected to be the closest, due to their common 13:30 daytime node Equatorial crossing time, and Terra to show slightly different magnitudes due to the diurnal variability of cloud cover (Eastman & Warren, 2014; Meskhidze et al., 2009). In much of the tropics and Australia, Terra coverage is higher due to early-afternoon formation of convective clouds and precipitation. In general, this retrieval availability fraction is closely linked to cloud cover, confirming this as the main limiting factor for such retrievals.

The VIIRS 3,040-km swath is sufficiently broad that consecutive orbits overlap, even at the Equator, while the narrower (but still quite broad) MODIS 2,330-km swaths have small gaps at the Equator but overlap at moderate and high latitudes. Additionally, the finer L2 resolution of VIIRS (nominal 6 versus 10 km and reduced bow-tie distortion) means that it should be easier for VIIRS to meet the requirement for at least three valid retrievals to populate a L3 daily grid cell. The first point in particular means it is expected that VIIRS would have slightly higher coverage than MODIS in tropical regions, and this is indeed seen to be the case. Over tropical deserts where cloud cover is low, coverage exceeds 75 % most of the time. VIIRS spatial coverage in general equals or exceeds that of MODIS Aqua in all regions.

At high northern latitudes, cloud/snow mean that coverage in all three data sets is much lower in December–May (25% or less) compared to June–November (~25–50%). VIIRS coverage is slightly higher (typically up to one 12.5% color bar increment) than that of MODIS Aqua at high latitudes in both hemispheres, although not enough to change the overall spatial pattern. While the additional potential views per day afforded by the broad swath are beneficial for increasing coverage, the major limiting factors (cloudiness, snow cover, and polar night) are persistent enough between orbits that they are not overcome by the more frequent revisits.



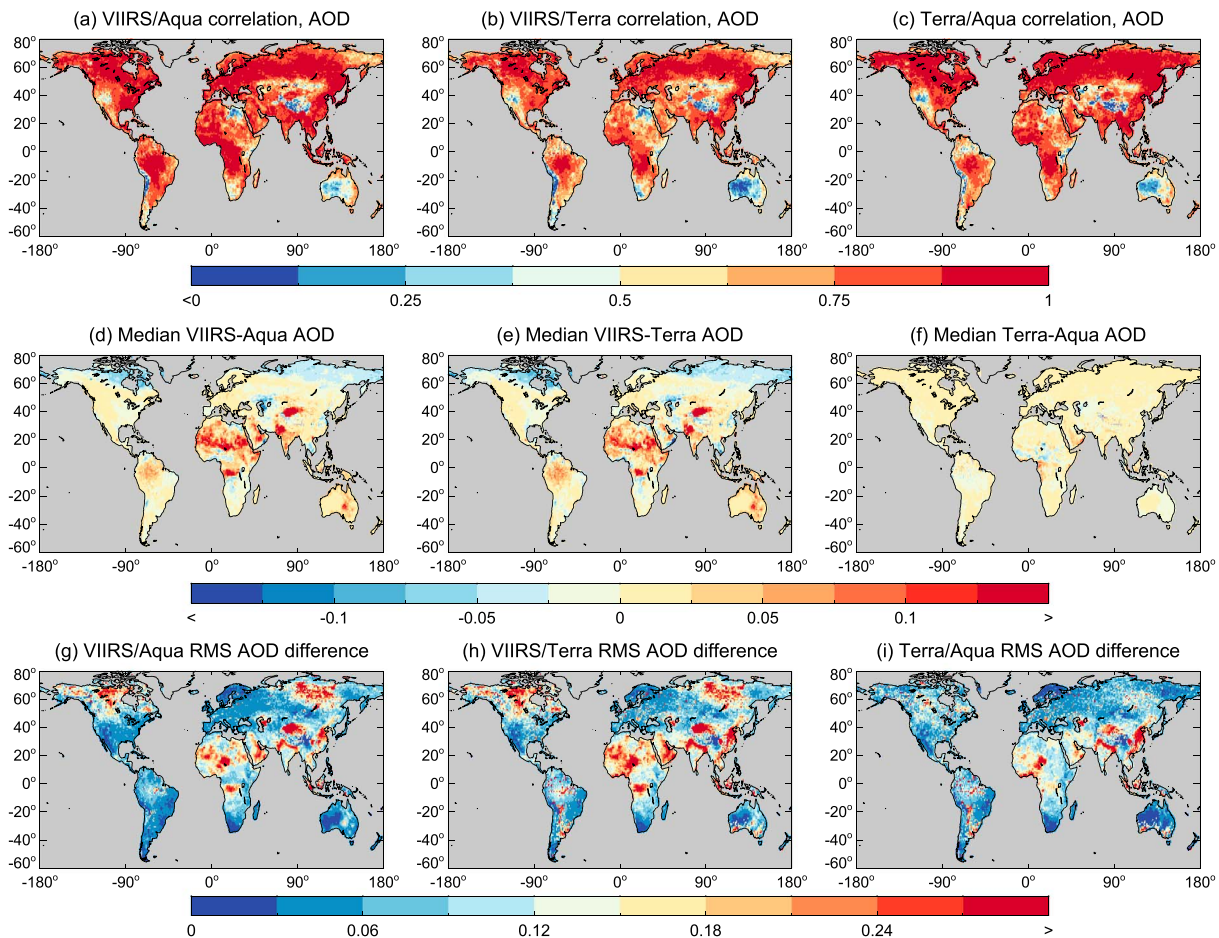


**Figure 16.** Statistics of intersensor AOD comparisons using D3 data from 2013–2015. From top–bottom, rows indicate (a–c) correlation, (d–f) offset (defined as first sensor minus second), and (g–i) RMS difference. From left–right, columns indicate VIIRS/MODIS Aqua, VIIRS/MODIS Terra, and MODIS Terra/MODIS Aqua. Grid cells with fewer than 10 valid days are shaded in gray.

#### 4.2. Statistics of Cosampled Data

Using the 3 years of D3 data, mapped statistics of each of the three pairwise comparisons between data sets are shown for AOD in Figure 16. These are calculated using only those daily grid cells where all three DB data sets provided data. Hereafter, V/A denotes the VIIRS versus MODIS Aqua pairing, V/T VIIRS versus MODIS Terra, and T/A MODIS Terra versus Aqua. For correlation, spatial patterns are similar for the three comparisons, and in general, correlation is high (0.75 or greater) for those regions which experience seasonal cycles in AOD or sporadic high-AOD events (e.g., isolated wildfires). Where correlation is low, such as in the Andes mountains, parts of Australia, and the Himalayas/Tibetan Plateau, AOD tends to be low and temporally fairly stable. Thus, the day-to-day variations which drive the correlation coefficient are small compared with small differences related to sampling and error characteristics. No one of the three comparisons shows uniformly stronger correlations.

The patterns for median offset and RMS difference show more variation. The smallest values are seen for T/A, likely due to the identical algorithm and sensor characteristics (the only differences being absolute calibration and orbit). For the source D3 matched data, 42% of points for this combination agree within  $\pm 0.02$ , increasing to 92% for the gridded median offsets shown in Figure 16. For V/A and V/T, these are 35% and 32% for the daily and 56% and 53% for the gridded median offsets, respectively, somewhat lower and largely driven by differences in well-sampled tropical and midlatitude deserts. For T/A, in most areas, Terra is slightly higher than Aqua; this was also observed by Levy et al. (2018), looking at DT retrieval results. Levy et al. (2018) investigated the magnitudes of calibration differences and diurnal variations on the Terra–Aqua offset and found that neither alone was responsible for it. DB uses some different bands and also applies 412- and 470-nm band calibration degradation corrections (Sayer, Hsu, Bettenhausen, Jeong, & Meister, 2015)



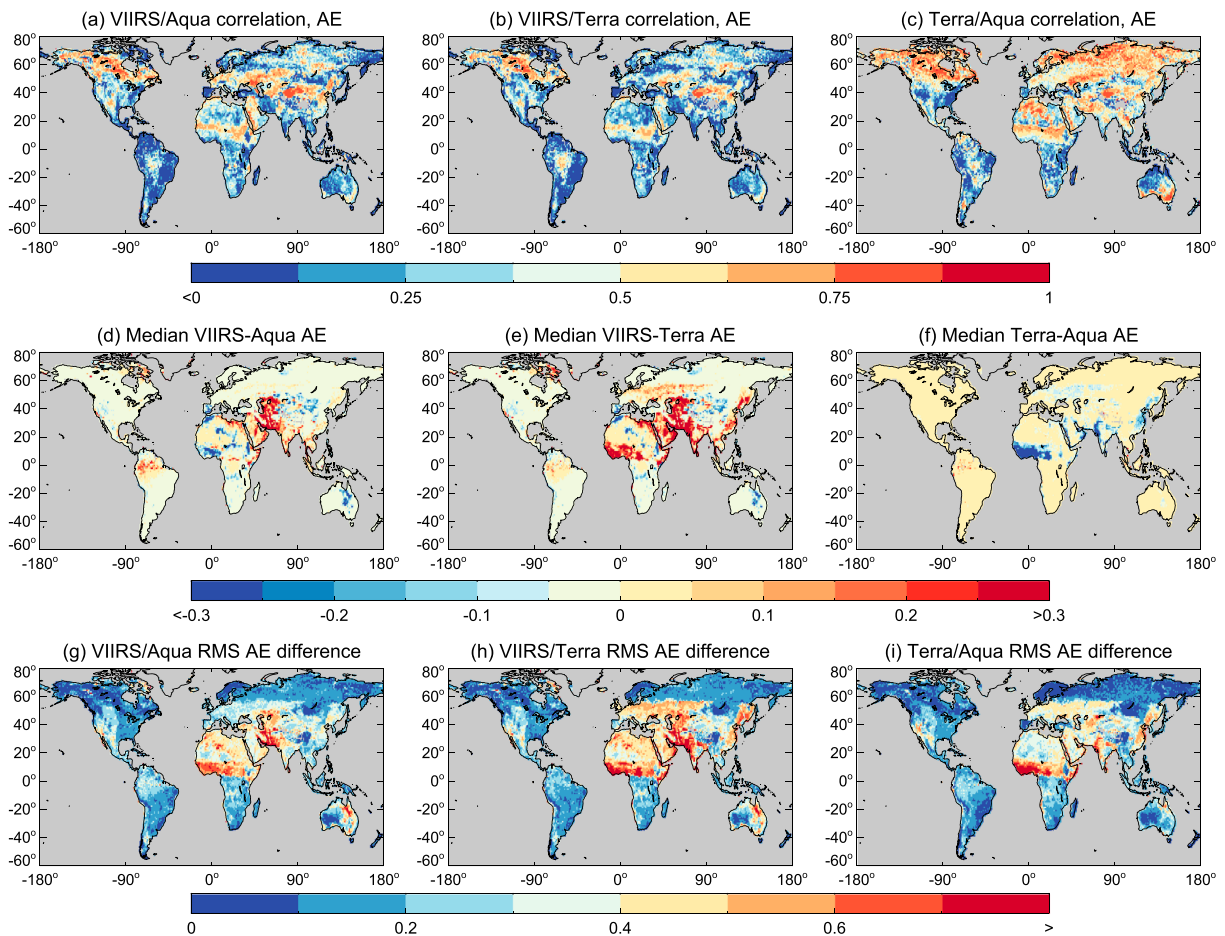


**Figure 17.** As Figure 16, except for AE.

which DT does not. The calibration part of that analysis may not be quantitatively transferable to DB because of this, although both algorithms also rely on other bands which may have unresolved absolute calibration differences.

Many of the areas where V/A and V/T show larger median differences than T/A are also those with higher RMS differences, parts of the Sahara and Arabian Peninsula, central Africa, the IGP, and Taklamakan desert. Those are regions in which aerosol/surface model updates were implemented in the VIIRS algorithm but were not able to be ported to MODIS before the code deadline for the C6.1 reprocessing (see section 3.3). The fact that V/A and V/T patterns are very similar indicate that sensor/algorithm differences are likely dominant, as opposed to diurnal variations. The reasons for lower VIIRS than MODIS AOD at high northern latitudes are uncertain but could be reflective of differences in pixel

selection near clouds, lakes, and snow due to sensor resolutions. The snow filter was also updated for VIIRS and not yet ported to MODIS, although as snow contamination tends to result in artificial hot spots of AOD, it is expected this update would lead to more isolated changes as opposed to a small large-scale offset. These scenes tend to be encountered at large solar zenith angles, and with these long path lengths, the effects of other sources (e.g., calibration differences, trace gas absorption, and surface models) can be accentuated. This region is almost entirely processed using the vegetated surface reflectance method (Figure 1), so sensor band differences (MODIS 470 nm vs. VIIRS 490 nm), which are the key wavelength used for the surface model here, are important. This will be investigated further for future DB reprocessings.

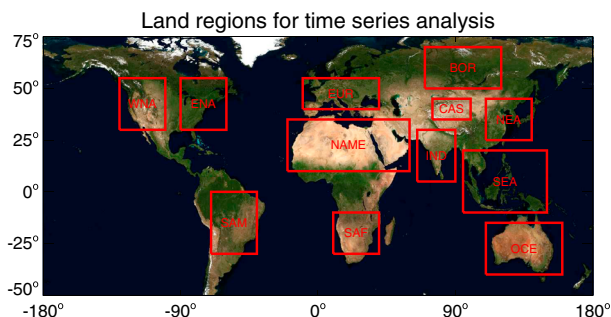


**Figure 18.** Regions used for the time series analysis in Figure 19 and Table 5.

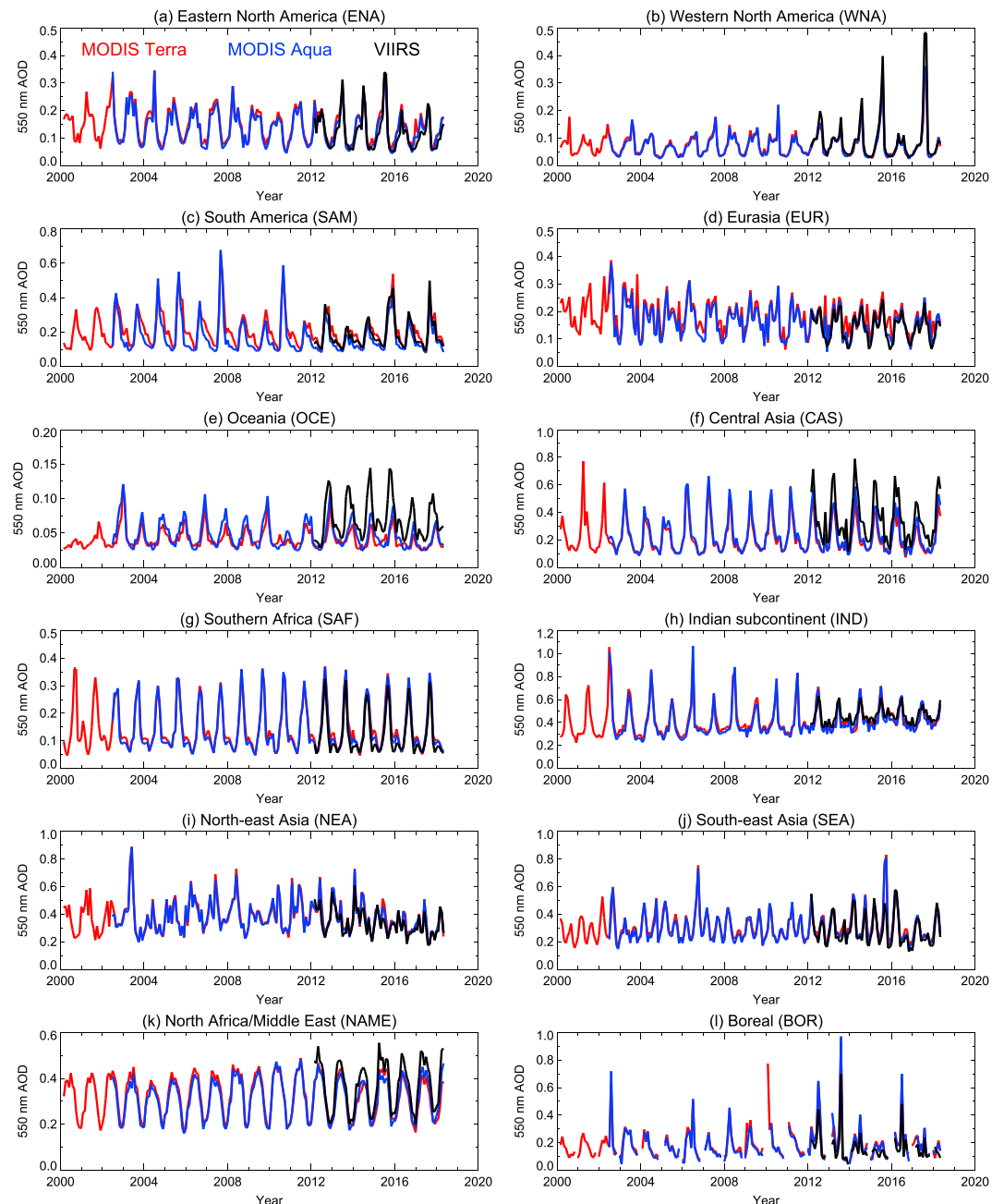


**Figure 19.** VIIRS, MODIS Terra, and MODIS Aqua monthly AOD time series for the regions shown in Figure 18.

Parts of Canada and Russia also show high RMS AOD differences in Figure 16, without large offsets. Examining these in more detail (not shown), the days contributing to the large RMS are mostly those affected by wildfires. These will also be investigated in the future, as there are many possible reasons why this could occur (calibration differences can have large effects when AOD is high; resolution differences and swath width differences can influence the number and spatial distribution of retrieval from which the D3 retrieval is computed).

Figure 17 provides equivalent results for AE. Similar general tendencies are seen as were observed for AOD, for the same reasons. Correlation, however, is somewhat lower: This is expected first due to the fact that it is a more uncertain retrieved parameter and second because much of the world is low-AOD much of the time, and in these cases AE is prescribed and not retrieved by DB (Hsu et al., 2013). These facts make interpretation of this figure somewhat difficult. The second factor means that large differences in AE may

be found dependent on whether or not a retrieval falls just or below this threshold for AE to be retrieved (AOD of 0.2 at 470 nm). Those places with a high correlation in AE tend to be ones where not only aerosol loading but also aerosol type change during the year, for example, high northern latitudes which alternate between clean background and heavy smoke and the Sahel which samples different combinations of dust and smoke aerosols at different times.

#### 4.3. Regional Time Series

The purpose of this section is to assess the consistency between the DB monthly mean time series on a regional basis. While L2 data sets are often used for case studies of individual events and for data assimilation applications, the M3 products are popular for time series analysis and comparison between different satellite and/or model data sets. Figure 18 shows the 12 regions chosen for this purpose; each is linked to one of the regions used for the AERONET validation analysis (cf. Figure 2), to provide further context, although the boundaries are adjusted to focus on particular aerosol features of interest and/or discrepancies seen in Figure 16. Section 3.3 discussed some of these regional aerosol features.

Figure 19 shows the resulting AOD time series, and Table 5 provides statistical metrics to assess the consistency between the data sets. In general, the time series reveal consistent magnitudes of AOD, including seasonality and interannual variability, and this is reflected in high correlations (excluding OCE) of 0.76–0.99, in most cases over 0.90. OCE is the exception again due to the aforementioned reason of low AOD and small temporal variability. For 10 of the 12 regions, the T/A correlation is the highest; for the other two (SAM and NAME), V/A is the highest, although in most of these cases, the difference in correlation is fairly small and probably not statistically significant. These high correlations indicate that all data sets represent basically the same seasonal and interannual variations of aerosol features.

For 10 of the 36 three-way matchups, the magnitude of the median offset between data sets is 0.01 or less, and for 21, it is 0.02 or less. The T/A offset is the smallest in 10 of 12 regions. V/T is expected to be more different from V/A due to the fact that sensor and overpass time are both different, and indeed, the V/A offset is smaller than V/T in eight regions. Likewise, the RMS difference is the smallest for T/A in 10 regions, and RMS difference for V/A is smaller than V/T in nine. Those regions with the largest differences between the three (in terms of offset and RMS) are the same as those with hot spots in Figure 16 (OCE, CAS, IND, and NAME).

For OCE, which here covers Australia, the difference is largely driven by higher VIIRS AOD in deserts and lake basins in eastern Australia. The offset is persistent year-round but appears largest from June–November. The CAS (here focused on the Taklamakan desert) and NAME (Sahara desert and Arabian Peninsula) regions also have year-round higher AOD in VIIRS; this is an intentional algorithm change in VIIRS to address a low bias in high-AOD dust events seen in MODIS C6 data. Despite the VIIRS offsets, these time series remain very strongly correlated (0.96–0.99 in CAS and 0.93–0.96 in NAME). Finally, as shown in Figures 6 and 16, changes in IND are due to higher VIIRS AOD in the IGP, ameliorating a low bias in previous versions of DB data. Correlation between the time series again remains high (0.89–0.97).

### 5. Conclusions and Future Perspective

The goal of DB is to create a long time series of aerosol properties from satellite measurements, by using data from similar sensor types and applying, as far as possible, the same retrieval techniques and assumptions. Through this principle, it is hoped that the resulting data sets will be sufficiently consistent to facilitate long-term time series analysis. The differences between the various instruments to which DB has been applied (AVHRR, SeaWiFS, MODIS, and VIIRS) introduce complications into attempts to create a long-term record. Sensor differences require algorithm adjustments and have consequences for sampling and error statistics. Orbital differences introduce complications due to, for example, the diurnal variation of aerosols and clouds, as well as solar/view geometries (which itself can affect algorithm performance). DB is to date the only AOD retrieval algorithm approach which has been implemented across this breadth of sensors.

It is unfortunate that there has not yet been long-term monitoring of the Earth in the visible to thermal infrared domain using an identical stable satellite sensor series. The AVHRRs all had slightly different spectral response functions, lacked onboard calibration, and their orbits drifted. Additionally, they have the fewest and broadest spectral bands. The two MODIS sensors are the most similar, although are on different orbits and have had unresolved calibration offsets. SeaWiFS is generally recognized as having the most

**Table 5***Correlation, Median Offset, and RMS Difference Between the Three Deep Blue Time Series for the Regions Shown in Figure 19*

| Region acronym and bounds        | Correlation |      |      | Offset |        |        | RMS difference |       |       |
|----------------------------------|-------------|------|------|--------|--------|--------|----------------|-------|-------|
|                                  | V/A         | V/T  | T/A  | V/A    | V/T    | T/A    | V/A            | V/T   | T/A   |
| ENA (30° N–55° N, 90° W–60° W)   | 0.92        | 0.92 | 0.98 | −0.013 | −0.018 | 0.010  | 0.025          | 0.032 | 0.014 |
| WNA (30° N–55° N, 130° W–100° W) | 0.97        | 0.96 | 0.99 | 0.006  | 0.006  | 0.002  | 0.027          | 0.032 | 0.006 |
| SAM (30° S–0° N, 70° W–40° W)    | 0.98        | 0.95 | 0.92 | 0.029  | −0.004 | 0.039  | 0.034          | 0.032 | 0.051 |
| EUR (40° N–55° N, 10° W–40° E)   | 0.91        | 0.76 | 0.95 | −0.008 | −0.023 | 0.012  | 0.021          | 0.042 | 0.025 |
| OCE (40° S–15° S, 110° E–160° E) | 0.79        | 0.58 | 0.83 | 0.020  | 0.024  | −0.005 | 0.033          | 0.038 | 0.010 |
| CAS (35° N–45° N, 75° E–100° E)  | 0.98        | 0.96 | 0.99 | 0.11   | 0.13   | −0.015 | 0.12           | 0.15  | 0.030 |
| SAF (30° S–10° S, 10° E–40° E)   | 0.95        | 0.89 | 0.98 | −0.018 | −0.020 | 0.003  | 0.024          | 0.031 | 0.013 |
| IND (5° N–30° N, 65° E–90° E)    | 0.90        | 0.89 | 0.97 | 0.048  | 0.027  | 0.021  | 0.059          | 0.050 | 0.031 |
| NEA (25° N–45° N, 110° E–140° E) | 0.95        | 0.93 | 0.98 | −0.011 | −0.010 | 0.004  | 0.045          | 0.052 | 0.020 |
| SEA (10° S–20° N, 95° E–150° E)  | 0.96        | 0.94 | 0.97 | −0.021 | −0.031 | 0.009  | 0.066          | 0.073 | 0.023 |
| NAME (10° N–35° N, 20° W–60° E)  | 0.98        | 0.93 | 0.96 | 0.046  | 0.054  | 0.012  | 0.056          | 0.065 | 0.022 |
| BOR (50° N–70° N, 70° E–120° E)  | 0.88        | 0.84 | 0.96 | −0.040 | −0.052 | 0.010  | 0.077          | 0.071 | 0.029 |

*Note.* ENA = Eastern North America; WNA = Western North America; SAM = South America; EUR = Europe; OCE = Oceania; CAS = Central Asia; SAF = Southern Africa; IND = Indian subcontinent; NEA = Northeastern Asia; SEA = Southeastern Asia; NAME = North Africa/Middle East; BOR = Boreal; T = Moderate Resolution Imaging Spectroradiometer Terra; A = Moderate Resolution Imaging Spectroradiometer Aqua; V = Visible Infrared Imaging Radiometer Suite; RMS = root mean square.

stable calibration (Franz et al., 2007) and had similar orbit characteristics to Aqua. However, it had more limited spatial resolution and coverage and lacked shortwave and thermal infrared bands, which affect cloud detection and dust identification capabilities. VIIRS on S-NPP is on a similar orbit to MODIS Aqua but also has differences in spatial resolution and available bands. It has therefore been impossible to obtain a truly consistent set of input measurements from which to construct such a record. One note of hope for the future is that successive VIIRS instruments, such as that launched on the NOAA20 platform in 2017 and an additional two to launch in the coming decades, should all be virtually identical in both sensor and orbital characteristics.

There is an inherent tension in that, as newer instruments become available, there is a desire to make use of sensor-specific improvements to improve the data records from individual sensors. In short, given different instrument specifications, making the fullest use of an individual sensor's capabilities increases the potential of loss of consistency with a less-capable sensor. The question of what level of difference is acceptable if one wants to consider data sets consistent with each other is strongly dependent on the particular application in question, and there is no one benchmark for consistency and continuity. Given the limitations of the available raw satellite measurements, the analysis in this study has attempted to answer the question of to what extent the latest versions of the MODIS and VIIRS DB algorithm can be regarded as consistent. Comparisons between different DB algorithm versions will be presented in more detail in a forthcoming algorithm paper. The ultimate judgment as to which data sets to use for a specific purpose will be up to the individual data user.

This analysis has been in terms of both error characteristics in comparison to AERONET as well as differences and time series on a regional scale. It has shown that, qualitatively and quantitatively, the AOD retrievals have similar expected levels of uncertainty of a little better (especially in low-AOD conditions) than  $\pm(0.05 + 20\%)$  versus AERONET overall and that the dependence of these errors on the context of the retrieval (i.e., stratified by surface type, aerosol loading, and aerosol type) are also similar. AE remains more qualitative than quantitative, but comparison statistics are again similar for the different data sets. Spatial and temporal variability of the data sets are also very similar. Analysis at long-term AERONET sites suggests a stability of order 0.01 per decade or better in AOD, with all sensors trending slightly upward through time. This stability meets GCOS requirements; continual monitoring of sensor calibration and stability of retrieval results is required to identify and remove residual trending as far as possible. The data also show strong qualitative and quantitative similarity in patterns of spatial coverage and in time series of AOD.



Due to external code delivery deadlines, the VIIRS V1 data set represents a slight advance on the MODIS Terra/Aqua C6.1 algorithm implementation. This results in some expected regional differences between the VIIRS and MODIS data sets, which are most notable over the Sahara Desert, Arabian Peninsula, Taklamakan Desert, and IGP. It is recommended that in the future reprocessings become synchronized as much as possible, to remove the possible confounding factors resulting from algorithm differences from analyses. Unexpected small negative and positive VIIRS-MODIS offsets are found for high northern latitudes and over Australia, respectively, and require further assessment.

The effects of sensor-specific differences are difficult to reduce, and impossible to entirely remove, from such attempts to create a long-term aerosol data record. Sensor absolute calibration is typically determined prelaunch via laboratory measurements, while on-orbit calibration is focused on stability and degradation via internal checks and/or observations of the Earth (Upřety et al., 2014) or Moon (Sun et al., 2007; Eplee et al., 2011). To bring separate sensors into absolute calibration alignment is complicated by the lack of a spaceborne on-orbit absolute calibration reference. Cross-calibration of sensors is possible, either directly against one another (Sayer, Hsu, Bettenhausen, et al., 2017) or through the use of the same ground targets (Franz et al., 2007; Lyapustin et al., 2014), although cannot provide the same level of confidence due to difficulties removing entirely the effects of geometric, spectral response, and trace gas absorption differences and radiative transfer model assumptions and limitations. It is vital that these efforts continue and remain possible for future sensors, to maintain the stability of individual records.

When algorithm and calibration differences have been minimized as far as possible, a further hurdle to be overcome lies in the optimal way to combine the various AOD records into one. This has not yet been addressed in detail within the aerosol remote sensing community, with most data records being single-sensor as opposed to merged. It may be that, rather than combining or comparing L3 daily/monthly time series, data fusion should begin on a L1b or L2 basis. The Multiangle Implementation of Atmospheric Correction algorithm (Lyapustin et al., 2011, 2018) is one step toward this, as it combines MODIS Terra and Aqua together at the L1b stage after cross-calibration corrections (Lyapustin et al., 2014). Bias correction and filtering techniques which have already been developed for DA purposes (e.g., Hyer et al., 2011; Zhang & Reid, 2010) could also be used to decrease errors and, hopefully, offsets between the data sets. To help overcome limitations related to diurnal variations in sampling and aerosol/cloud motion, DB could also be applied to geostationary measurements to provide a transfer standard. The new generation of geostationary instruments have more MODIS-like spectral, spatial, and radiometric capabilities and disk image revisit times typically of order 15 min or less. These “blended” approaches have been successful at creating merged multisensor products for geophysical quantities such as surface temperature (Banzon et al., 2016), clouds (Rossow & Schiffer, 1999), and precipitation (Huffman et al., 2007).

## Acknowledgments

More information about the Deep Blue aerosol project, including further documentation and links, can be found online (<https://deepblue.gsfc.nasa.gov>). This research was funded by NASA's radiation science programme, managed by Hal Maring. The Atmosphere SIPS at the University of Wisconsin are thanked for VIIRS data processing. Work at the Atmosphere SIPS is being performed for NASA under contract NNG15HZ38C. AERONET data are available online (<https://aeronet.gsfc.nasa.gov>); the AERONET team and site Principal Investigators and managers are thanked for the creation and maintenance of the AERONET data record, which is central to the continued assessment of remotely sensed and modeled aerosol data sets. MODIS and VIIRS data are available from the NASA LAADS (<https://ladsweb.nascom.nasa.gov>), who are thanked for hosting the data. GTOPO30 was obtained from the USGS Land Processes Distributed Active Archive Center (LP DAAC), located at USGS/EROS, Sioux Falls, SD (<http://lpdaac.usgs.gov>). A. Lyapustin and one anonymous reviewer are thanked for their comments and suggestions, which helped improve the clarity of this manuscript. The authors declare no conflicts of interest.

## References

- Abdullaev, S. F., Maslow, V. A., Nazarow, I., & Salikhov, T. K. (2014). Variations in parameters of aerosol optical thickness in Dushanbe. *Izvestiya, Atmospheric and Oceanic Physics*, 50(4), 431–424.
- Banzon, V., Smith, T. M., Chin, T. M., Liu, C., & Hankins, W. (2016). A long-term record of blended satellite and in situ sea-surface temperature for climate monitoring, modeling and environmental studies. *Earth System Science Data*, 8, 165–176. <https://doi.org/10.5194/essd-8-165-2016>
- Barnes, W. L., Pagano, T. S., & Salomonson, V. V. (1998). Pre-launch characteristics of the Moderate Resolution Imaging Spectroradiometer (MODIS) on EOS-AM1. *IEEE Transactions on Geoscience and Remote Sensing*, 36(4), 1088–1100. <https://doi.org/10.1109/36.700993>
- Cao, C., Xiong, J., Blonski, S., Liu, Q., Upřety, S., Shao, X., & Weng, F. (2013). Suomi NPP VIIRS sensor data record verification, validation, and long-term performance monitoring. *Journal of Geophysical Research: Atmospheres*, 118, 11,664–11,678. <https://doi.org/10.1002/2013JD020418>
- Chew, B. N., Campbell, J. R., Reid, J. S., Giles, D. M., Welton, E. J., Salinas, S. V., & Liew, S. C. (2011). Tropical cirrus cloud contamination in Sun photometer data. *Atmospheric Environment*, 45(37), 6724–6731. <https://doi.org/10.1016/j.atmosenv.2011.08.017>
- Chin, M., Diehl, T., Tan, Q., Prospero, J. M., Kahn, R. A., Remer, L. A., et al. (2014). Multi-decadal aerosol variations from 1980 to 2009: A perspective from observations and a global model. *Atmospheric Chemistry and Physics*, 14, 3657–3690. <https://doi.org/10.5194/acp-14-3657-2014>
- Chubarova, N. E., Gorbarenko, E. V., Nezval', E. I., & Shilovtseva, O. A. (2011). Aerosol and radiation characteristics of the atmosphere during forest and peat fires in 1972, 2002, and 2010 in the Region of Moscow. *Izvestiya, Atmospheric and Oceanic Physics*, 47(6), 729–738. <https://doi.org/10.1134/S0001433811060028>
- Damoah, R., Spichtinger, N., Forster, C., James, P., Mattis, I., Wandinger, U., & Stohl, A. (2004). Around the world in 17 days-hemispheric-scale transport of forest fire smoke from Russia in May 2003. *Atmospheric Chemistry and Physics*, 4, 1311–1321. <https://doi.org/10.5194/acp-4-1311-2004>
- Dey, S., & Di Girolamo, L. (2011). A decade of change in aerosol properties over the Indian subcontinent. *Geophysical Research Letters*, 38, L14811. <https://doi.org/10.1029/2011GL048153>



- Dubovik, O., Holben, B., Eck, T. F., Smirnov, A., Kaufman, Y., King, M., & Slutsker, I. (2002). Variability and optical properties of key aerosol types observed in worldwide locations. *Journal of Atmospheric Sciences*, 59, 590–608. [https://doi.org/10.1175/1520-0469\(2002\)059<0590:VOAAOP>2.0.CO;2](https://doi.org/10.1175/1520-0469(2002)059<0590:VOAAOP>2.0.CO;2)
- Eastman, R., & Warren, S. G. (2014). Diurnal cycles of cumulus, cumulonimbus, stratus, stratocumulus, and fog from surface observations over land and ocean. *Journal of Climate*, 27, 2386–2404. <https://doi.org/10.1175/JCLI-D-13-00352.1>
- Eck, T. F., Holben, B. N., Reid, J. S., Dubovik, O., Smirnov, A., O'Neill, N. T., & Kinne, S. (1999). Wavelength dependence of the optical depth of biomass burning, urban, and desert dust aerosols. *Journal of Geophysical Research*, 104(D24), 31,333–31,349.
- Eck, T. F., Holben, B. N., Reid, J. S., Mukelabai, M. M., Pikheth, S. J., Torres, O., & Slutsker, I. (2013). A seasonal trend of single scattering albedo in southern African biomass-burning particles: Implications for satellite products and estimates of emissions for the world's largest biomass-burning source. *Journal of Geophysical Research: Atmospheres*, 118, 6414–6432. <https://doi.org/10.1002/jgrd.50500>
- Eck, T. F., Holben, B. N., Reid, J. S., O'Neill, N. T., Schafer, J. S., Dubovik, O., & Artaxo, P. (2003). High aerosol optical depth biomass burning events: A comparison of optical properties for different source regions. *Geophysical Research Letters*, 30(20), 2035. <https://doi.org/10.1029/2003GL017861>
- Eck, T. F., Holben, B. N., Reid, J. S., Sinyuk, A., Hyer, E. J., O'Neill, N. T., & Newcomb, W. W. (2009). Optical properties of boreal region biomass burning aerosols in central Alaska and seasonal variation of aerosol optical depth at an Arctic coastal site. *Journal of Geophysical Research*, 114, D11201. <https://doi.org/10.1029/2008JD010870>
- Eplee, R. E. Jr, Sun, J. Q., Meister, G., Patt, F. S., Xiong, C. R., & McClain, X. (2011). Cross calibration of SeaWiFS and MODIS using on-orbit observations of the Moon. *Applied Optics*, 50(2), 120–133. <https://doi.org/10.1364/AO.50.000120>
- Field, R. D., van der Werd, G. R., Fanin, T., Fetzner, E. J., Fuller, R., Jethva, H., & Worden, H. M. (2016). Indonesian fire activity and smoke pollution in 2015 show persistent nonlinear sensitivity to El Niño-induced drought. *Proceedings of the National Academy of Sciences*, 113(33), 9204–9209. <https://doi.org/10.1073/pnas.1524888113>
- Franz, B. A., Bailey, S. W., Werdell, P. J., & McClain, C. R. (2007). Sensor-independent approach to the vicarious calibration of satellite ocean color radiometry. *Applied Optics*, 46(22), 5068–5082. <https://doi.org/10.1364/AO.46.005068>
- GCOS (2011). Systematic observation requirements for satellite-based data products for climate, 2011 update. Retrieved from [https://library.wmo.int/doc\\_num.php?explnum\\_id=3710](https://library.wmo.int/doc_num.php?explnum_id=3710) (World Meteorological Organization (WMO) Global Climate Observing System (GCOS) report GCOS-154)
- Gautam, R., Hsu, N. C., Eck, T. F., Holben, B. N., Janjai, S., Jantarach, T., & Lau, W. K. (2013). Characterization of aerosols over the Indochina peninsula from satellite-surface observations during biomass burning pre-monsoon season. *Atmospheric Environment*, 78, 51–59. <https://doi.org/10.1016/j.atmosenv.2012.05.038>
- Gautam, R., Hsu, N. C., Tsay, S. C., Lau, W. K., Holben, B., Bell, S., & Kim, K. M. (2011). Accumulation of aerosols over the Indo-Gangetic plains and southern slopes of the Himalayas: Distribution, properties and radiative effects during the 2009 pre-monsoon season. *Atmospheric Chemistry and Physics*, 11, 12841–12863. <https://doi.org/10.5194/acp-11-12841-2011>
- Gesch, D. B., & Larson, K. S. (1996). Techniques for development of global 1-kilometer digital elevation models. In *Pecora Thirteen Human Interactions with the Environment-Perspectives from Space*, U.S.
- Gesch, D. B., Verdin, K. L., & Greenlee, S. K. (1999). New land surface digital elevation model covers the Earth. *Eos, Transactions, American Geophysical Union*, 80(6), 69–70. <https://doi.org/10.1029/99EO00050>
- Giles, D. M., Sinyuk, A., Sorokin, M. G., Schafer, J. S., Smirnov, A., Slutsker, I., & Lyapustin, A. I. (2019). Advancements in the Aerosol Robotic Network (AERONET) version 3 database automated near-real-time quality control algorithm with improved cloud screening for Sun photometer aerosol optical depth (AOD) measurements. *Atmospheric Measurement Techniques*, 12, 169–209. <https://doi.org/10.5194/amt-12-169-2019>
- Ginoux, P., Prospero, J. M., Gill, T. E., Hsu, N. C., & Zhao, M. (2012). Global-scale attribution of anthropogenic and natural dust sources and their emission rates based on MODIS Deep Blue aerosol products. *Reviews of Geophysics*, 50, RG3005. <https://doi.org/10.1029/2012RG000388>
- Heald, C. L., Ridley, D. A., Kroll, J. H., Barrett, S. R. H., Cady-Pereira, K. E., Alvarado, M. J., & Holmes, C. D. (2014). Contrasting the direct radiative effect and direct radiative forcing of aerosols. *Atmospheric Chemistry and Physics*, 14, 5513–5527. <https://doi.org/10.5194/acp-14-5513-2014>
- Henriksson, S. V., Laaksonen, A., Kerminen, V. M., Räisänen, P., Järvinen, H., Sundström, A. M., & de Leeuw, G. (2011). Spatial distributions and seasonal cycles of aerosols in India and China seen in global climate-aerosol model. *Atmospheric Chemistry and Physics*, 11, 7975–7990. <https://doi.org/10.5194/acp-11-7975-2011>
- Holben, B. N., Eck, T. F., Slutsker, I., Tanré, D., Buis, J. P., Setzer, A., & Smirnov, A. (1998). AERONET: A federated instrument network and data archive for aerosol characterization. *Remote Sensing of Environment*, 66, 1–16. [https://doi.org/10.1016/S0034-4257\(98\)00031-5](https://doi.org/10.1016/S0034-4257(98)00031-5)
- Hsu, N. C., Jeong, M. J., Bettenhausen, C., Sayer, A. M., Hansell, R., Seftor, C. S., & Tsay, S. C. (2013). Enhanced Deep Blue aerosol retrieval algorithm: The second generation. *Journal of Geophysical Research: Atmospheres*, 118, 9296–9315. <https://doi.org/10.1002/jgrd.50712>
- Hsu, N. C., Lee, J., Sayer, A. M., Carletta, N., Chen, S. H., Tucker, C. J., & Tsay, S. C. (2017). Retrieving near-global aerosol loading over land and ocean from AVHRR. *Journal of Geophysical Research: Atmospheres*, 122, 9968–9989. <https://doi.org/10.1002/2017JD026932>
- Hsu, N. C., Tsay, S. C., King, M. D., & Herman, J. R. (2004). Aerosol properties over bright-reflecting source regions. *IEEE Transactions on Geoscience and Remote Sensing*, 42(3), 557–569. <https://doi.org/10.1109/TGRS.2004.824067>
- Hsu, N. C., Tsay, S. C., King, M. D., & Herman, J. R. (2006). Deep Blue retrievals of Asian aerosol properties during ACE-Asia. *IEEE Transactions on Geoscience and Remote Sensing*, 44(11), 3180–3195. <https://doi.org/10.1109/TGRS.2006.879540>
- Huang, J., Hsu, N. C., Tsay, S. C., Jeong, M. J., Holben, B. N., Berkoff, T. A., & Welton, E. J. (2011). Susceptibility of aerosol optical thickness retrievals to thin cirrus contamination during the BASE-ASIA campaign. *Journal of Geophysical Research*, 116, D08214. <https://doi.org/10.1029/2010JD014910>
- Huffman, G. J., Bolvin, D. T., Nelkin, E. J., Wolff, D. B., Adler, R. F., Gu, G., & Stocker, E. F. (2007). The TRMM Multisatellite Precipitation Analysis (TMPA): Quasi-global, multiyear, combined-sensor precipitation estimates at fine scales. *Journal of Hydrometeorology*, 8(1), 38–55. <https://doi.org/10.1175/JHM560.1>
- Hyer, E. H., Reid, J. S., & Zhang, J. (2011). An over-land aerosol optical depth data set for data assimilation by filtering, correction, and aggregation of MODIS Collection 5 optical depth retrievals. *Atmospheric Measurement Techniques*, 4, 379–408. <https://doi.org/10.5194/amt-4-379-2011>
- Ichoku, C., Chu, D. A., Mattoo, S., Kaufman, Y. J., Remer, L. A., Tanré, D., & Holben, B. N. (2002). A spatio-temporal approach for global validation and analysis of MODIS aerosol products. *Geophysical Research Letters*, 29(12), 1616. <https://doi.org/10.1029/2001GL013206>
- Jeong, M. J., Hsu, N. C., Kwiatkowska, E. J., Franz, B. A., Meister, G., & Salustro, C. E. (2011). Impacts of cross-platform vicarious calibration on the Deep Blue aerosol retrievals for Moderate Resolution Imaging Spectroradiometer aboard Terra. *IEEE Transactions on Geoscience and Remote Sensing*, 49(12), 4877–4988. <https://doi.org/10.1109/TGRS.2011.2153205>

- Kaufman, Y. J., Wald, A. E., Remer, L. A., Gao, B. C., Li, R. R., & Flynn, L. (1997). The MODIS 2.1  $\mu\text{m}$  channel-correlation with visible reflectance for use in remote sensing of aerosol. *IEEE Transactions on Geoscience and Remote Sensing*, 35(5), 1286–1298. <https://doi.org/10.1109/36.628795>
- Koren, I., Kaufman, Y., Washington, R., Todd, M. C., Rudich, Y., Martins, J. V., & Rosenfeld, D. (2006). The Bodélé depression: A single spot in the Sahara that provides most of the mineral dust to the Amazon forest. *Environmental Research Letters*, 1, 14005.
- Levy, R. C., Mattoo, S., Sawyer, V., Shi, Y., Colarco, P. R., Lyapustin, A. I., & Remer, L. A. (2018). Exploring systematic offsets between aerosol products from the two MODIS sensors. *Atmospheric Measurement Techniques*, 11, 4073–4092. <https://doi.org/10.5194/amt-11-4073-2018>
- Levy, R. C., Remer, L. A., Kleidman, R. G., Mattoo, S., Ichoku, C., Kahn, R., & Eck, T. F. (2010). Global evaluation of the Collection 5 MODIS dark-target aerosol products over land. *Atmospheric Chemistry and Physics*, 10, 10,399–10,420. <https://doi.org/10.5194/acp-10-10399-2010>
- Levy, R. C., Remer, L. A., Mattoo, S., Vermote, E. F., & Kaufman, Y. J. (2007). Second-generation operational algorithm: Retrieval of aerosol properties over land from inversion of Moderate Resolution Imaging Spectroradiometer spectral reflectance. *Journal of Geophysical Research*, 112, D13211. <https://doi.org/10.1029/2006JD007811>
- Lyapustin, A., Wang, Y., Korkin, S., & Huang, D. (2018). MODIS Collection 6 MAIAC algorithm. *Atmospheric Measurement Techniques*, 11, 5741–5765. <https://doi.org/10.5194/amt-11-5741-2018>
- Lyapustin, A., Wang, Y., Laszlo, I., Kahn, R., Korkin, S., Remer, L., & Reid, J. S. (2011). Multiangle Implementation of Atmospheric Correction (MAIAC): 2. Aerosol algorithm. *Journal of Geophysical Research*, 116, D03211. <https://doi.org/10.1029/2010JD014986>
- Lyapustin, A., Wang, Y., Xiong, X., Meister, G., Platnick, S., Levy, R., & Angal, A. (2014). Scientific impact of MODIS C5 calibration degradation and C6+ improvements. *Atmospheric Measurement Techniques*, 7, 4353–4365. <https://doi.org/10.5194/amt-7-4353-2014>
- McFarquhar, G. M., Heymsfield, A. J., Spinhirne, J., & Hart, B. (2000). Thin and subvisual tropopause tropical cirrus: Observations and radiative impacts. *Journal of the Atmospheric Sciences*, 57(12), 1841–1853. [https://doi.org/10.1175/1520-0469\(2000\)057<1841:TASTTC>2.0.CO;2](https://doi.org/10.1175/1520-0469(2000)057<1841:TASTTC>2.0.CO;2)
- Meister, G., & Franz, B. A. (2011). Adjustments to the MODIS Terra radiometric calibration and polarization sensitivity in the 2010 reprocessing. *Proceedings of SPIE*, 8153, 1–12. <https://doi.org/10.1117/12.891787>
- Meister, G., Kwiatkowska, E. J., Franz, B. A., Patt, F. S., Feldman, G. C., & McClain, C. R. (2005). Moderate-Resolution Imaging Spectroradiometer ocean color polarization correction. *Applied Optics*, 44(26), 5524–5535. <https://doi.org/10.1364/AO.44.005524>
- Meskhidze, N., Remer, L. A., Platnick, S., Negrón Juárez, R., Lichtenberger, A. M., & Aiyer, A. R. (2009). Exploring the differences in cloud properties observed by the Terra and Aqua MODIS Sensors. *Atmospheric Chemistry and Physics*, 9, 3461–3475. <https://doi.org/10.5194/acp-9-3461-2009>
- Moeller, C., Grey, R., Borbas, E., Menzel, W. P., Wilson, T., Wu, A., & Geng, X. (2017). Improvements to Terra MODIS L1B, L2, and L3 science products through using crosstalk corrected L1B radiances. In *Proceedings of SPIE*, 10402, Earth Observing Systems XXII. San Diego, CA. <https://doi.org/10.1117/12.2274340>
- Negi, B. S., Sadasivan, S., & Mishra, U. C. (1967). Aerosol composition and sources in urban areas in India. *Atmospheric Environment*, 21(6), 1259–1266. [https://doi.org/10.1016/0004-6981\(67\)90072-8](https://doi.org/10.1016/0004-6981(67)90072-8)
- Pandithurai, G., Pinker, R. T., Dubovik, O., Holben, B. N., & Aro, T. (2001). Remote sensing of aerosol optical characteristics in sub-Sahel, West Africa. *Journal of Geophysical Research*, 106(D22), 28,347–28,356. <https://doi.org/10.1029/2001JD900234>
- Parekh, P. P., Ghauri, B., Siddiqi, Z. R., & Husain, L. (1967). The use of chemical and statistical methods to identify sources of selected elements in ambient air aerosols in Karachi, Pakistan. *Atmospheric Environment*, 21(6), 1267–1274. [https://doi.org/10.1016/0004-6981\(67\)90073-X](https://doi.org/10.1016/0004-6981(67)90073-X)
- Park, S. S., Kim, Y. J., Cho, S. Y., & Kim, S. J. (2007). Characterization of PM<sub>2.5</sub> aerosols dominated by local pollution and Asian dust observed at an urban site in Korea during Aerosol Characterization Experiments (ACE) Asia Project. *Journal of the Air & Waste Management Association*, 57(4), 434–443. <https://doi.org/10.3155/1047-3289.57.4.434>
- Popp, T., De Leeuw, G., Bingen, C., Brühl, C., Capelle, V., Chedin, A., et al. (2016). Development, production and evaluation of Aerosol Climate Data Records from European Satellite Observations (Aerosol\_cci). *Remote Sensing*, 8, 5. <https://doi.org/10.3390/rs8050421>
- Prospero, J. M., Collard, F. X., Molinié, J., & Jeannot, A. (2014). Characterizing the annual cycle of African dust transport to the Caribbean Basin and South America and its impact on the environment and air quality. *Global Biogeochemical Cycles*, 29, 757–773. <https://doi.org/10.1002/2013GB004802>
- Qin, Y., & Mitchell, R. M. (2009). Characterisation of episodic aerosol types over the Australian continent. *Atmospheric Chemistry and Physics*, 9, 1943–1956. <https://doi.org/10.5194/acp-9-1943-2009>
- Rahot, J. L. (2008). AMMA dust experiment: An overview of measurements performed during the dry season special observation period (SOP0) at the Banizoumbou (Niger) supersite. *Journal of Geophysical Research*, 113, D00C14. <https://doi.org/10.1029/2008JD009906>
- Reid, J. S., Eck, T. F., Christopher, S. A., Koppmann, R., Dubovik, O., Eleuterio, D. P., & Zhang, J. (2005). A review of biomass burning emissions part III: Intensive optical properties of biomass burning particles. *Atmospheric Chemistry and Physics*, 5, 827–849. <https://doi.org/10.5194/acp-5-827-2005>
- Reid, J. S., Hyer, E. J., Johnson, R. S., Holben, B. N., Yokelson, R. J., Zhang, J., & Liew, S. C. (2013). Observing and understanding the Southeast Asian aerosols system by remote sensing: An initial review and analysis for the Seven Southeast Asian Studies (7 SEAS) program. *Atmospheric Research*, 122, 303–468. <https://doi.org/10.1016/j.atmosres.2012.06.005>
- Reid, J. S., Koppmann, R., Eck, T. F., & Eleuterio, D. P. (2005). A review of biomass burning emissions part II: Intensive physical properties of biomass burning particles. *Atmospheric Chemistry and Physics*, 5, 799–825. <https://doi.org/10.5194/acp-5-799-2005>
- Remer, L. A., Kleidman, R. G., Levy, R. C., Kaufman, Y. J., Tanré, D., Mattoo, S., & Holben, B. N. (2008). Global aerosol climatology from the MODIS satellite sensors. *Journal of Geophysical Research*, 113, D14S07. <https://doi.org/10.1029/2007JD009661>
- Ridley, D. A., Heald, C. L., Kok, J. F., & Zhao, C. (2016). An observationally constrained estimate of global dust aerosol optical depth. *Atmospheric Chemistry and Physics*, 16, 15,097–15,117. <https://doi.org/10.5194/acp-16-15097-2016>
- Rizzo, L. V., Artaxo, P., Müller, T., Wiedensohler, A., Paixão, M., Cirino, G. G., & Kulmala, M. (2013). Long term measurements of aerosol optical properties at a primary forest site in Amazonia. *Atmospheric Chemistry and Physics*, 13, 2391–2413. <https://doi.org/10.5194/acp-13-2391-2013>
- Roberts, G., Wooster, M. J., & Lagoudakis, E. (2009). Annual and diurnal African biomass burning temporal dynamics. *Biogeosciences*, 6, 849–866. <https://doi.org/10.5194/bg-6-849-2009>
- Rosow, W. B., & Schiffer, R. A. (1999). Advances in understanding clouds from ISCCP. *Bulletin of the American Meteorological Society*, 80(11), 2261–2288. [https://doi.org/10.1175/1520-0477\(1999\)080<2261:AIUCFI>2.0.CO;2](https://doi.org/10.1175/1520-0477(1999)080<2261:AIUCFI>2.0.CO;2)
- Salinas, S. V., Chew, B. N., Mohamad, N., & Liew, S. C. (2013). First measurements of aerosol optical depth and Angstrom exponent number from AERONET's Kuching site. *Atmospheric Environment*, 78, 231–241. <https://doi.org/10.1016/j.atmosenv.2013.02.016>

- Sayer, A. M., Hsu, N. C., & Bettenhausen, C. (2015). Implications of MODIS bow-tie distortion on aerosol optical depth retrievals, and techniques for mitigation. *Atmospheric Measurement Techniques*, 8, 5277–5288. <https://doi.org/10.5194/amt-8-5277-2015>
- Sayer, A. M., Hsu, N. C., Bettenhausen, C., Ahmad, Z., Holben, B. N., Smirnov, A., & Zhang, J. (2012). SeaWiFS Ocean Aerosol Retrieval (SOAR): Algorithm, validation, and comparison with other data sets. *Journal of Geophysical Research*, 117, D03206. <https://doi.org/10.1029/2011JD016599>
- Sayer, A. M., Hsu, N. C., Bettenhausen, C., Holz, R. E., Lee, J., Quinn, G., & Veglio, P. (2017). Cross-calibration of S-NPP VIIRS moderate-resolution reflective solar bands against MODIS Aqua over dark water scenes. *Atmospheric Measurement Techniques*, 10, 1425–1444. <https://doi.org/10.5194/amt-10-1425-2017>
- Sayer, A. M., Hsu, N. C., Bettenhausen, C., & Jeong, M. J. (2013). Validation and uncertainty estimates for MODIS Collection 6 “Deep Blue” aerosol data. *Journal of Geophysical Research: Atmospheres*, 118, 7864–7872. <https://doi.org/10.1002/jgrd.50600>
- Sayer, A. M., Hsu, N. C., Bettenhausen, C., Jeong, M. J., Holben, B. N., & Zhang, J. (2012). Global and regional evaluation of over-land spectral aerosol optical depth retrievals from SeaWiFS. *Atmospheric Measurement Techniques*, 5, 1761–1778. <https://doi.org/10.5194/amt-5-1761-2012>
- Sayer, A. M., Hsu, N. C., Bettenhausen, C., Jeong, M. J., & Meister, G. (2015). Effect of MODIS Terra radiometric calibration improvements on Collection 6 Deep Blue aerosol products: Validation and Terra/Aqua consistency. *Journal of Geophysical Research: Atmospheres*, 120, 12,157–12,174. <https://doi.org/10.1002/2015JD023878>
- Sayer, A. M., Hsu, N. C., Eck, T. F., Smirnov, A., & Holben, B. N. (2014). AERONET-based models of smoke-dominated aerosol near source regions and transported over oceans, and implications for satellite retrievals of aerosol optical depth. *Atmospheric Chemistry and Physics*, 14, 11,493–11,523. <https://doi.org/10.5194/acp-14-11493-2014>
- Sayer, A. M., Hsu, N. C., Lee, J., Bettenhausen, C., Kim, W. V., & Smirnov, A. (2018). Satellite Ocean Aerosol Retrieval (SOAR) algorithm extension to S-NPP VIIRS as part of the Deep Blue aerosol project. *Journal of Geophysical Research: Atmospheres*, 123, 380–400. <https://doi.org/10.1002/2017JD027412>
- Sayer, A. M., Hsu, N. C., Lee, J., Carletta, N., Chen, S. H., & Smirnov, A. (2017). Evaluation of NASA Deep Blue/SOAR aerosol retrieval algorithms applied to AVHRR measurements. *Journal of Geophysical Research: Atmospheres*, 122, 9945–9967. <https://doi.org/10.1002/2017JD026934>
- Sayer, A. M., Munchak, L. A., Hsu, N. C., Levy, R. C., Bettenhausen, C., & Jeong, M. J. (2014). MODIS Collection 6 aerosol products: Comparison between Aqua’s e-Deep Blue, Dark Target, and merged data sets, and usage recommendations. *Journal of Geophysical Research: Atmospheres*, 119, 13,965–13,989. <https://doi.org/10.1002/2014JD022453>
- Schuster, G. L., Dubovik, O., & Holben, B. N. (2006). Angstrom exponent and bimodal aerosol size distributions. *Journal of Geophysical Research*, 111, D07207. <https://doi.org/10.1029/2005JD006328>
- Sharma, R. K., Bhattarai, B. K., Sapkota, B. K., Gewali, M. B., & Kjeldstad, B. (2012). Black carbon aerosols variation in Kathmandu Valley, Nepal. *Atmospheric Environment*, 63, 282–288. <https://doi.org/10.1016/j.atmosenv.2012.09.023>
- Smirnov, A., Holben, B. N., Eck, T. F., Dubovik, O., & Slutsker, I. (2000). Cloud-screening and quality control algorithms for the AERONET database. *Remote Sensing Environment*, 73(3), 337–349.
- Sogacheva, L., de Leeuw, G., Rodriguez, E., Kolmonen, P., Georgoulas, A. K., Alexandri, G., & van der, A. R. J. (2018). Spatial and seasonal variations of aerosols over China from two decades of multi-satellite observations. Part I: ATSR (1995–2011) and MODIS C6.1 (2000–2017). *Atmospheric Chemistry and Physics*, 18, 11,389–11,407. <https://doi.org/10.5194/acp-18-11389-2018>
- Sun, J., Xiong, X., Barnes, W., & Guenther, B. (2007). MODIS reflective solar bands on-orbit lunar calibration. *IEEE Transactions on Geoscience and Remote Sensing*, 45(7), 2383–2393. <https://doi.org/10.1109/TGRS.2007.896541>
- Tanré, D., Kaufman, Y. J., Herman, M., & Mattoo, S. (1997). Remote sensing of aerosol properties over oceans using the MODIS/EOS spectral radiances. *Journal of Geophysical Research*, 102(D14), 16,971–16,988. <https://doi.org/10.1029/96JD03437>
- Toller, G. X., Xiong, X. J., Sun, J., Wenny, B. N., Geng, X., Kuypers, J., & Wu, A. (2013). Terra and Aqua Moderate-Resolution Imaging Spectroradiometer collection 6 level 1B algorithm. *Journal of Applied Remote Sensing*, 7(1), 73557. <https://doi.org/10.1117/1.JRS.7.073557>
- Turquety, S., Logan, J. A., Jacob, D. J., Hudman, R. C., Leung, F. Y., Heald, C. L., & Sachse, G. W. (2007). Inventory of boreal fire emissions for North America in 2004: Importance of peat burning and pyroconvective injection. *Journal of Geophysical Research*, 112, D12S03. <https://doi.org/10.1029/2006JD007281>
- Upreti, S., Cao, C., Blonski, S., & Wang, W. (2014). Assessment of VIIRS radiometric performance using vicarious calibration sites. In *Proceedings of SPIE*, 9218. San Diego, CA. <https://doi.org/10.1117/12.2061855>
- van Donkelaar, A., Martin, R. V., Braur, M., Hsu, N. C., Kahn, R. A., Levy, R. C., & Winker, D. M. (2016). Global estimates of fine particulate matter using a combined geophysical-statistical method with information from satellites, models, and monitors. *Environmental Science and Technology*, 50(7), 3762–3772. <https://doi.org/10.1021/acs.est.5b05833>
- van der Werf, G. R., Randerson, J. T., Giglio, L., Collatz, G. J., Mu, M., Kasibhatla, P. S., & van Leeuwen, T. T. (2010). Global fire emissions and the contribution of deforestation, savanna, forest, agricultural, and peat fires (1997–2009). *Atmospheric Chemistry and Physics*, 10, 11,707–11,735. <https://doi.org/10.5194/acp-10-11707-2010>
- Virtanen, T. H., Kolmonen, P., Sogacheva, L., Rodríguez, E., Saponaro, G., & de Leeuw, G. (2018). Collocation mismatch uncertainties in satellite aerosol retrieval validation. *Atmospheric Measurement Techniques*, 11, 925–938. <https://doi.org/10.5194/amt-11-925-2018>
- Wagner, F., & Silva, A. M. (2008). Some considerations about Ångström exponent distributions. *Atmospheric Chemistry and Physics*, 8, 481–489. <https://doi.org/10.5194/acp-8-481-2008>
- Wang, X., Cheng, H., Che, H., Sun, J., Lu, H., Qiang, M., & Li, D. (2017). Modern dust aerosol availability in northwestern China. *Eos, Transactions, American Geophysical Union*, 7, 8741. <https://doi.org/10.1038/s41598-017-09458-w>
- Weatherhead, E. C., Tiao, G. C., Meng, X. L., Choi, D., & Cheang, W. K. (1998). Factors affecting the detection of trends: Statistical considerations and applications to environmental data. *Journal of Geophysical Research*, 103(D14), 17,149–17,161. <https://doi.org/10.1029/98JD00995>
- Wolfe, R. E., Lin, G., Tewari, K. P., Tilton, J. C., & Isaacman, A. R. (2013). Suomi NPP VIIRS prelaunch and on-orbit geometric calibration and characterization. *Journal of Geophysical Research: Atmospheres*, 118, 11,508–11,521. <https://doi.org/10.1002/jgrd.50873>
- Xiong, X., Butler, J., Chiang, K., Efremova, B., Fulbright, J., Lei, N., & Wu, A. (2016). Assessment of S-NPP VIIRS on-orbit radiometric calibration and performance. *Remote Sens.*, 8, 1–9. <https://doi.org/10.3390/rs8020084>
- Xiong, X., Che, N., Barnes, W., Xie, X., Wang, L., & Qu, J. (2006). Status of Aqua MODIS spatial characterization and performance. In *Proceedings of SPIE*, 6361, *Sensors, Systems, and Next-Generation Satellites X*. <https://doi.org/10.1117/12.687162>
- Zhang, J., & Reid, J. S. (2010). A decadal regional and global trend analysis of the aerosol optical depth using a data-assimilation grade over-water MODIS and Level 2 MISR aerosol products. *Atmospheric Chemistry and Physics*, 10, 10,949–10,963. <https://doi.org/10.5194/acp-10-10949-2010>